sequencing using an ABI PRISM 3100 genetic analyzer (ABI Advanced Biotechnologies, Columbia, MD). Oligonucleotide primers and PCR conditions used for amplification of all exons 1–53 of *ABCA12* were originally derived from the report by Lefèvre *et al.* (2003) and were partially modified for the present study. The entire coding region including the exon/intron boundaries for both forward and reverse strands from the patient, family members, and 100 healthy Japanese controls were sequenced. No mutations were found in 200 normal alleles from the healthy Japanese population. Paternity testing was carried out using 16 microsatellite markers. The parents provided informed consent to the experiments. The experiments received institutional approval and the protocol adhered to The Declaration of Helsinki Principles.

Ultrastructural observations

Skin biopsy samples were fixed in 5% glutaraldehyde solution, post-fixed in 1% OsO_4, dehydrated, and embedded in Epon 812. The samples were sectioned at 1 μm thickness for light microscopy and thin sectioned for electron microscopy (70 nm thick). The thin sections were stained with uranyl acetate and lead citrate and examined in a transmission electron microscope. As controls, lesional skin samles from lamellar ichthyosis patients with transglutaminase 1 gene mutations (Akiyama *et al.*, 2001) or *ABCA12* mutations were also studied.

Cell culture

A skin sample from the patient was processed for primary keratinocyte culture, and cells were grown according to standard procedures in defined keratinocyte serum-free medium (Invitrogen Corp., Carlsbad, CA). After several passages in low-Ca^{2+} (0.09 mM) conditions, cultures were grown in high-Ca^{2+} (2.0 mM) conditions.

Antibodies

Polyclonal anti-ABCA12 antiserum was raised in rabbits using a 14 amino-acid sequence synthetic peptide (residues 2567–2580) derived from the ABCA12 sequence (NM 173076) as the immunogen (Akiyama *et al.*, 2005). The other primary antibody was mouse monoclonal anti-glucosylceramide antibody (Alexis Biochemicals, Lausanne, Switzerland).

Immunofluorescent labeling

Immunofluorescent labeling was performed as previously described (Akiyama *et al.*, 2000). Briefly, 6-μm-thick sections of fresh patient's skin was cut using a cryostat. The sections were incubated in primary antibody solution for 1 hour at 37°C. Antibody dilutions were as follows; 1/10 for anti-ABCA12 antiserum and 1/10 for anti-glucosylceramide antibody. The sections were then incubated in FITC-conjugated to rabbit anti-mouse Igs and tetramethylrhodamine isothiocyanate-conjugated goat anti-rabbit Igs diluted 1:100 (DAKO, Glostrup, Denmark) for 30 minutes at room temperature, followed by nuclear counterstain by TO-PRO-3 (Invitrogen, Carlsbad, CA). The sections were extensively washed with phosphate-buffered saline between incubations. The stained sections were then mounted with a cover slip and observed using a confocal laser scanning microscope.

CONFLICT OF INTEREST
The authors state no conflict of interest.

ACKNOWLEDGMENTS
We thank Ms Megumi Sato, Ms Maki Goto and Ms Akari Nagasaki for their fine technical assistance on this project. This work was supported in part by Grant-in-Aid from the Ministry of Education, Science, Sports, and Culture of Japan to M. Akiyama (Kiban B 16390312).

REFERENCES

Akiyama M (1999) The pathogenesis of severe congenital ichthyosis of the neonate. *J Dermatol Sci* 21:96–104

Akiyama M (in press a) Pathomechanisms of harlequin ichthyosis and ABC transporters in human diseases. *Arch Dermatol*

Akiyama M (in press b) Harlequin ichthyosis and other autosomal recessive congenital ichthyoses: the underlying genetic defects and pathomechanisms. *J Dermatol Sci*

Akiyama M, Sawamura D, Nomura Y, Sugawara M, Shimizu H (2003) Truncation of CGI-58 protein causes malformation of lamellar granules resulting in ichthyosis in Dorfman–Chanarin syndrome. *J Invest Dermatol* 121:1029–34

Akiyama M, Sugiyama-Nakagiri Y, Sakai K, McMillan JR, Goto M, Arita K *et al.* (2005) Mutations in ABCA12 in harlequin ichthyosis and functional rescue by corrective gene transfer. *J Clin Invest* 115:1777–84

Akiyama M, Smith LT, Shimizu H (2000) Changing patterns of localization of putative stem cells in developing human hair follicles. *J Invest Dermatol* 114:321–7

Akiyama M, Takizawa Y, Suzuki Y, Ishiko A, Matsuo I, Shimizu H (2001) Compound heterozygous TGM1 mutations including a novel missense mutation L204Q in a mild form of lamellar ichthyosis. *J Invest Dermatol* 116:992–5

Allikmets R, Gerrard B, Hutchinson A, Dean M (1996) Characterization of the human ABC superfamily: isolation and mapping of 21 new genes using the expressed sequence tags database. *Hum Mol Genet* 5:1649–55

Allikmets R, Singh N, Sun H, Shroyer NF, Hutchinson A, Chidambaram A *et al.* (1997a) A photoreceptor cell-specific ATP-binding transporter gene (ABCR) is mutated in recessive Stargardt macular dystrophy. *Nat Genet* 15:236–46

Allikmets R, Shroyer NF, Singh N, Seddon JM, Lewis RA, Bernstein PS *et al.* (1997b) Mutation of the Stargardt disease gene (ABCR) in age-related macular degeneration. *Science* 277:1805–7

Annilo T, Shulenin S, Chen ZQ, Arnould I, Prades C, Lemoine C *et al.* (2002) Identification and characterization of a novel ABCA subfamily member, ABCA12, located in the lamellar ichthyosis region on 2q34. *Cytogenet Genome Res* 98:169–76

Borst P, Elferink RO (2002) Mammalian ABC transporters in health and disease. *Annu Rev Biochem* 71:537–92

Brooks-Wilson A, Marcil M, Clee SM, Zhang LH, Roomp K, van Dam M *et al.* (1999) Mutations in ABC1 in Tangier disease and familial high-density lipoprotein deficiency. *Nat Genet* 22:336–45

Dean M, Rzhetsky A, Allikmets R (2001) The human ATP-binding cassette (ABC) transporter superfamily. *Genome Res* 11:1156–66

Hayden MR, Clee SM, Brooks-Wilson A, Genest J Jr, Attie A, Kastelein JJ (2000) Cholesterol efflux regulatory protein, Tangier disease and familial high-density lipoprotein deficiency. *Curr Opin Lipidol* 11:117–22

Higgins CF (1992) ABC transporters: from microorganisms to man. *Annu Rev Cell Biol* 8:67–113

Holleran WM, Takagi Y, Menon GK, Legler G, Feingold KR, Elias PM (1993) Processing of epidermal glucosylceramides is required for optimal mammalian cutaneous permeability barrier function. *J Clin Invest* 91:1656–64

Ishida-Yamamoto A, Simon M, Kishibe M, Miyauchi Y, Takahashi H, Yoshida S *et al.* (2004) Epidermal lamellar granules transport different cargoes as distinct aggregates. *J Invest Dermatol* 122:1137–44

Judge MR, McLean WHI, Munro CS (2004) Disorders of keratinization. In: *Rook/Wilkinson/Ebling: Textbook of Dematology.* (Burns T, Breathnach S, Cox N, Griffiths C, eds), Oxford, UK: Blackwell Science, 34.1–11

Kelsell DP, Norgett EE, Unsworth H, The M-T, Cullup T, Mein CA *et al.* (2005) Mutations in ABCA12 underlie the severe congenital skin disease harlequin ichthyosis. *Am J Hum Genet* 76:794–803

Klein I, Sarkadi B, Varadi A (1999) An inventory of the human ABC proteins. *Biochim Biophys Acta* 1461:237–62

Lefèvre C, Audebert S, Jobard F, Bouadjar B, Lakhdar H, Boughdene-Stambouli O *et al.* (2003) Mutations in the transporter ABCA12 are associated with lamellar ichthyosis type 2. *Hum Mol Genet* 12:2369–78

Lefèvre C, Bouadjar B, Ferrand V, Tadini G, Mégarbané A, Lathrop M *et al.* (2006) Mutations in a new cytochrome P450 gene in lamellar ichthyosis type 3. *Hum Mol Genet* 15:767–76

Oram JF (2002) Molecular basis of cholesterol homeostasis: lessons from Tangier disease and ABCA1. *Trends Mol Med* 8:168–73

Orso E, Broccardo C, Kaminski WE, Bottcher A, Liebisch G, Drobnik W *et al.* (2000) Transport of lipids from Golgi to plasma membrane is defective in tangier disease patients and Abc1-deficient mice. *Nat Genet* 24:192–6

Peelman F, Labeur C, Vanloo B, Roosbeek S, Devaud C, Duverger N *et al.* (2003) Characterization of the ABCA transporter subfamily: identification of prokaryotic and eukaryotic members, phylogeny and topology. *J Mol Biol* 325:259–74

Rust S, Rosier M, Funke H, Real J, Amoura Z, Piette JC *et al.* (1999) Tangier disease is caused by mutations in the gene encoding ATP-binding cassette transporter 1. *Nat Genet* 22:352–5

Schmitz G, Langmann T (2001) Structure, function and regulation of the ABC1 gene product. *Curr Opin Lipidol* 12:129–40

Shibaki A, Akiyama M, Shimizu H (2004) Novel ALDH3A2 heterozygous mutations are associated with defective lamellar granule formation in a Japanese family of Sjögren–Larsson syndrome. *J Invest Dermatol* 123: 1197–9

Uitto J (2005) The gene family of ABC transporters – novel mutations, new phenotypes. *Trends Mol Med* 11:341–3

Vielhaber G, Pfeiffer S, Brade L, Lindner B, Goldmann T, Vollmer E *et al.* (2001) Localization of ceramide and glucosylceramide in human epidermis by immunogold electron microscopy. *J Invest Dermatol* 117: 1126–36

Weng J, Mata NL, Azarian SM, Tzekov RT, Birch DG, Travis GH (1999) Insights into the function of Rim protein in photoreceptors and etiology of Stargardt's disease from the phenotype in abcr knockout mice. *Cell* 98: 13–23

Williams ML, Elias PM (1987) Genetically transmitted, generalized disorders of cornification; the ichthyoses. *Dermatol Clin* 5:155–78

Gene Corner

A novel *ABCA12* mutation 3270delT causes harlequin ichthyosis

DOI: 10.1111/j.1365-2133.2006.07434.x

Harlequin ichthyosis (HI) is a severe and often fatal congenital ichthyosis with an autosomal recessive inheritance pattern.[1] The clinical features include thick, plate-like scales with ectropion, eclabium, and flattened ears. The skin development is altered in utero.[2] *ABCA12* mutations have been reported to underlie HI[3,4] and it was clarified that HI is caused by severe functional defects in the keratinocyte lipid transporter ABCA12.[3] The pathomechanism of HI lies in the defective function of the lipid transporter ABCA12 which causes abnormal lipid lamellar granule transport in the keratinocytes, and results in a malformation of the epidermal lipid barrier.[3] Until the 1980s, newborns affected with HI rarely survived beyond the neonatal period. However, recently, HI babies have often had a better prognosis.[5–7] It is still unclear whether the good prognosis in HI is due to some remnant ABCA12 protein transporter function in the patients or not. Here, we report a girl with HI with a novel homozygous *ABCA12* deletion mutation leading to a complete loss of function of ABCA12, who has survived despite having severe ichthyosis showing the clinical features of nonbullous congenital ichthyosiform erythroderma (NBCIE).

Case and methods

The patient is the first child of healthy, unrelated German parents. There was no positive family history of any related disorders. The baby girl was born after premature rupture of the amnion in the 34th week of pregnancy (weight 1930 g, length 43 cm, head circumference 32 cm). The skin of the newborn was covered with large, thick, white, diamond-shaped plaques, partly bordered by irregular, bleeding fissures (Fig. 1). Hands and feet were oedematous, the tips of the fingers and toes were white with tight skin, and mobility in all joints was reduced.

After therapy with oral retinoids and local application of carbamide and emollient ointment, in a humid incubator, the hyperkeratosis detached within 2–6 weeks and passive and spontaneous mobility increased. The oedema and skin tightness also decreased. During infancy, the patient showed white to grey scales on her erythematous trunk skin, extremities and face (Fig. 2). Now, at age 8 years, she is doing well with continuous therapy with emollient ointment, vitamin D_3 and iodide and the avoidance of sunlight, although she still has severe ichthyosis with several features of NBCIE. Her mental status is normal, and she attends the second grade of a normal school. At age 8 years the patient is 114 cm tall (below third percentile), demonstrating that growth development is delayed.

Mutational analysis of *ABCA12* was performed in the affected baby, her parents and her healthy sisters. Briefly, genomic DNA isolated from peripheral blood cells was subjected to polymerase chain reaction (PCR) amplification, followed by direct automated sequencing using an ABI PRISM 3100 Genetic Analyzer (ABI Advanced Biotechnologies, Columbia, MD, U.S.A.). Oligonucleotide primers and PCR conditions used for amplification of all exons 1–53 of *ABCA12* were originally derived from the report by Lefèvre et al.[8] and were partially modified for the present study. The entire coding region including the exon/intron boundaries for both forward and reverse strands from the patient, family members and 100 healthy controls was sequenced.

Biopsy samples from the patient's ichthyotic skin were fixed in 5% glutaraldehyde solution, postfixed in 1% OsO_4, dehydrated, and embedded in Epon 812. The samples were sectioned at 1 μm thickness for light microscopy and thin sectioned for electron microscopy (70 nm thick). The thin sections were stained with uranyl acetate and lead citrate and examined in a transmission electron microscope.

Results and discussion

Mutation analysis of the 53 exons including the exon/intron boundaries of the entire *ABCA12* gene revealed a homozygous deletion mutation 3270delT in exon 23 in the patient (sequence according to Lefèvre et al.;[8] GenBank NM173076; Fig. 3). The mutation was verified as present in a heterozygous fashion in her parents and a sister (Fig. 3). Another sister carried no mutations. The mutation was not found in sequence analysis of 200 alleles from 100 normal, unrelated individuals, and therefore is unlikely to be a polymorphism (data not shown). The deletion mutation 3270delT leads to a frameshift and introduces a stop codon at codon 1090, within the first transmembrane domain complex of the ABCA12 protein.[9] Thus, the homozygous deletion mutation results in a truncation of ABCA12 peptide with the loss of both ATP-binding cassettes (ABCs), and is thought to have a serious effect on the function of the ABCA12 protein.

Skin biopsy showed compact, severe hyperkeratosis. Electron microscopy revealed numerous abnormal lamellar

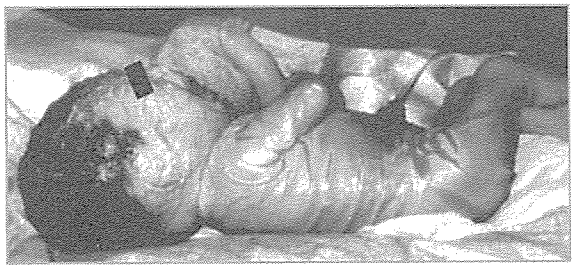

Fig 1. The patient showed the typical clinical phenotype of harlequin ichthyosis in the neonatal period. The entire body surface was covered with thick plate-like scales and fissures. Her auricles were malformed.

granules in the granular layer keratinocytes and accumulation of extruded irregular lamellar granules as vesicular structures, either empty or filled with glycogen-like particles between the epidermal cornified cells.

The ABC transporter superfamily is one of the largest gene families, encoding a highly conserved group of proteins involved in energy-dependent (active) transport of a variety of substrates across membranes.[10,11] The ABCA subfamily, of which the *ABCA12* gene is a member, is assumed to be involved in lipid transport.[12] Mutations in these genes underlie several human genetic diseases.[7,13] In 2005 it was reported that *ABCA12* mutations underlie HI,[3,4] and we showed that serious *ABCA12* mutations cause abnormal lipid transport via lamellar granules in keratinocytes, resulting in the malformation or improper assembly of the epidermal keratinocyte surface lipid barrier and the HI phenotype.[3] Recently, the long-term survival of patients with HI has been more frequently observed and documented,[3–7,14] despite HI having been considered to be an almost invariably fatal disorder until as recently as the 1980s. In the present patient with HI, the underlying *ABCA12* mutation, 3270delT, results in the truncation of the ABCA12 peptide at codon 1090 within the first transmembrane domain complex. Thus, the causative mutation leads to a loss of both ABCs and is thought to lead to a loss of ABCA12 function. Therefore, our homozygous patient is predicted to have an absence of ABCA12 transporter activity. However, our patient survived beyond the perinatal and neonatal period, probably in part due to the oral retinoid treatment. She is now 8 years old and her general condition is good without the need for retinoid treatment, although she

Fig 2. Clinical features at 3 years of age. The entire skin surface (A) was erythematous and covered with grey-white to grey scales, including the hands (B) and feet (C).

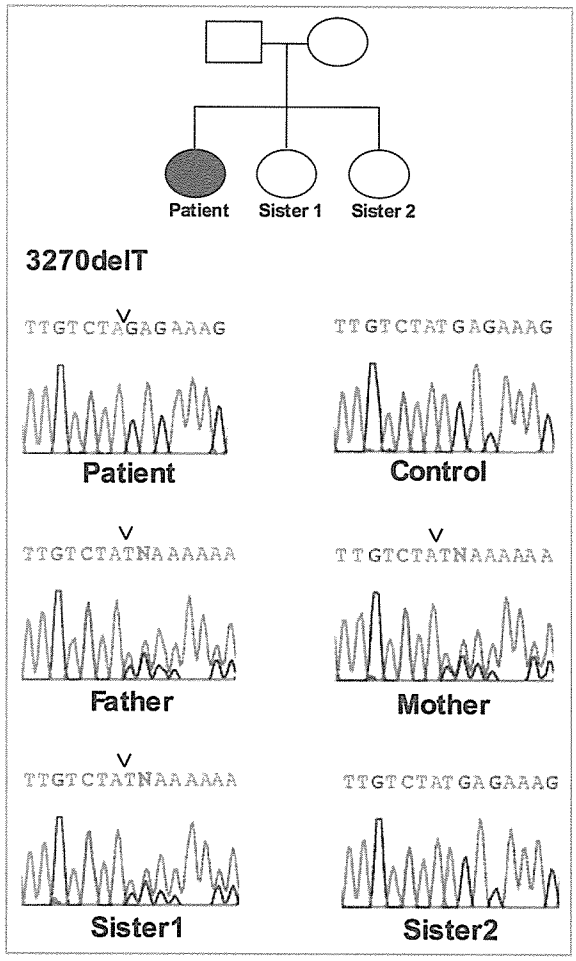

Fig 3. Homozygous mutation of *ABCA12* in the patient. The pedigree of the patient's family (top). Direct sequencing revealed a homozygous 3270delT (changing tyrosine residue at codon 1090 to a stop codon) in exon 23 of *ABCA12* of the patient. In both parents and one sister, the deletion mutation was found in a heterozygous state. The mutation was not present in the other sister or in the control samples.

has the clinical features of NBCIE over her entire body. This case may suggest that a patient with HI can survive beyond the perinatal and neonatal period with oral retinoid treatment, even if the causative *ABCA12* mutation leads to a complete loss of function of ABCA12. Further accumulation of similar cases is needed to confirm the effect of systemic retinoid on the prognosis of HI.

Acknowledgments

We thank Ms Maki Goto and Ms Akari Nagasaki for their fine technical assistance on this project. This work was supported in part by Grant-in-Aid from the Ministry of Education, Science, Sports, and Culture of Japan to M.A. (Kiban B 16390312 and Kiban B 18390310).

Department of Dermatology, Hokkaido University Graduate School of Medicine, North 15 West 7, Kita-ku, Sapporo 060-8638, Japan — M. Akiyama, K. Sakai
Institut für Humangenetik und Anthropologie, Albert-Ludwigs-Universität Freiburg, Freiburg, Germany — G. Wolff
†Department of Dermatology, University Clinic Heidelberg, Heidelberg, Germany — I. Hausser†
‡Creative Research Institute Sousei, Hokkaido University, Sapporo, Japan — J.R. McMillan‡, D. Sawamura, H. Shimizu
E-mail: akiyama@med.hokudai.ac.jp

References

1 Akiyama M. Harlequin ichthyosis and other autosomal recessive congenital ichthyoses: the underlying genetic defects and pathomechanisms. *J Dermatol Sci* 2006; **42**:83–9.
2 Akiyama M, Dale BA, Smith LT *et al.* Regional difference in expression of characteristic abnormality of harlequin ichthyosis in affected fetuses. *Prenat Diagn* 1998; **18**:425–36.
3 Akiyama M, Sugiyama-Nakagiri Y, Sakai K *et al.* Mutations in *ABCA12* in harlequin ichthyosis and functional rescue by corrective gene transfer. *J Clin Invest* 2005; **115**:1777–84.
4 Kelsell DP, Norgett EE, Unsworth H *et al.* Mutations in *ABCA12* underlie the severe congenital skin disease harlequin ichthyosis. *Am J Hum Genet* 2005; **76**:794–803.
5 Elias PM, Fartasch M, Crumrine D *et al.* Origin of the corneocyte lipid envelope (CLE): observations in harlequin ichthyosis and cultured human keratinocytes. *J Invest Dermatol* 2000; **115**:765–9.
6 Singh S, Bhura M, Maheshwari A *et al.* Successful treatment of harlequin ichthyosis with acitretin. *Int J Dermatol* 2001; **40**:472–3.
7 Akiyama M. Pathomechanisms of harlequin ichthyosis and ABC transporters in human diseases. *Arch Dermatol* (in press).
8 Lefèvre C, Audebert S, Jobard F *et al.* Mutations in the transporter *ABCA12* are associated with lamellar ichthyosis type 2. *Hum Mol Genet* 2003; **12**:2369–78.
9 Annilo T, Shulenin S, Chen ZQ *et al.* Identification and characterization of a novel ABCA subfamily member, *ABCA12*, located in the lamellar ichthyosis region on 2q34. *Cytogenet Genome Res* 2002; **98**:169–76.
10 Borst P, Elferink RO. Mammalian ABC transporters in health and disease. *Annu Rev Biochem* 2002; **71**:537–92.
11 Uitto J. The gene family of ABC transporters – novel mutations, new phenotypes. *Trends Mol Med* 2005; **11**:341–3.
12 Peelman F, Labeur C, Vanloo B *et al.* Characterization of the ABCA transporter subfamily: identification of prokaryotic and eukaryotic members, phylogeny and topology. *J Mol Biol* 2003; **325**:259–74.
13 Klein I, Sarkadi B, Varadi A. An inventory of the human ABC proteins. *Biochim Biophys Acta* 1999; **1461**:237–62.
14 Akiyama M, Sakai K, Sugiyama-Nakagiri Y *et al.* Compound heterozygous mutations including a *de novo* missense mutation in *ABCA12* led to a case of harlequin ichthyosis with moderate clinical severity. *J Invest Dermatol* 2006; **126**:1518–23.

Accepted for publication 3 May 2006

Key words: ABCA12 mutation, ATP-binding cassette transporter, harlequin ichthyosis, lipid transporter, retinoid, truncation

Conflicts of interest: None declared.

The American Journal of Pathology, Vol. 169, No. 2, August 2006

DOI: 10.2353/ajpath.2006.051242

Epithelial and Mesenchymal Cell Biology

A Novel N14Y Mutation in Connexin26 in Keratitis-Ichthyosis-Deafness Syndrome

Analyses of Altered Gap Junctional Communication and Molecular Structure of N Terminus of Mutated Connexin26

Ken Arita,* Masashi Akiyama,*
Tomoyasu Aizawa,† Yoshitaka Umetsu,†
Ikuo Segawa,‡ Maki Goto,* Daisuke Sawamura,*
Makoto Demura,† Keiichi Kawano,† and
Hiroshi Shimizu*

From the Department of Dermatology, Hokkaido University Graduate School of Medicine, Sapporo, Japan; Laboratory of Structural Bio-Macromolecular Science III,† Division of Biological Science, Hokkaido University, Sapporo, Japan; and the Department of Dermatology,‡ Iwate Prefectural Central Hospital, Iwate, Japan*

Connexins (Cxs) are transmembranous proteins that connect adjacent cells via channels known as gap junctions. The N-terminal 21 amino acids of Cx26 are located at the cytoplasmic side of the channel pore and are thought to be essential for the regulation of channel selectivity. We have found a novel mutation, N14Y, in the N-terminal domain of Cx26 in a case of keratitis-ichthyosis-deafness syndrome. Reduced gap junctional intercellular communication was observed in the patient's keratinocytes by the dye transfer assay using scrape-loading methods. The effect of this mutation on molecular structure was investigated using synthetic N-terminal peptides from both wild-type and mutated Cx26. Two-dimensional ^{1}H nuclear magnetic resonance and circular dichroism measurements demonstrated that the secondary structures of these two model peptides are similar to each other. However, several novel nuclear Overhauser effect signals appeared in the N14Y mutant, and the secondary structure of the mutant peptide was more susceptible to induction of 2,2,2-trifluoroethanol than wild type. Thus, it is likely that the N14Y mutation induces a change in local structural flexibility of the N-terminal domain, which is important for exerting the activity of the channel function, resulting in impaired gap junctional intercellular communication. *(Am J Pathol 2006, 169:416–423; DOI: 10.2353/ajpath.2006.051242)*

Gap junctions are involved in cell-cell attachment of almost all tissues, including the skin. Their most characteristic function is that of an intercellular channel. Gap junctions are made up of connexins (Cxs), transmembranous proteins that transverse the cell membrane four times, with their N and C termini located on the cytoplasmic side of the membrane. Cxs form tube-like hexamer structures, called connexons, that aggregate to the cell membrane and to connexons of opposite cells, forming gap junctional plaques. Through gap junctions, certain ions and second messengers less than 1 kd can pass from cell to cell. Thereby, gap junctions play important roles in cell-cell communication and tissue homeostasis.[1,2]

The importance of gap junctional intercellular communication in the function of several tissues or organs is demonstrated by the presence of Cx gene mutations in several congenital disorders.[1,2] For example, Cx26 mutations are a major cause of nonsyndromic congenital sensorineural deafness (DFNB1: MIM no. 220290). The Cx-related deafness is sometimes associated with congenital skin disorders, such as Vohwinkel's syndrome (MIM no. 124500)[3] and keratitis-ichthyosis-deafness (KID) syndrome (MIM no. 148210).[4] These syndromic deafness syndromes are autosomal dominant diseases in which it is assumed that the mutated Cx26 protein inhibits normal gap junction function by a dominant-negative effect.[5]

Supported in part by the Ministry of Education, Science, Sports, and Culture of Japan (Kiban B grant-in-aid 16390312 to M.A.).

Accepted for publication April 25, 2006.

Address reprint requests to Ken Arita, Department of Dermatology, Hokkaido University Graduate School of Medicine, North 15 West 7, Kita-ku, Sapporo 060-8638, Japan. E-mail: ariken@med.hokudai.ac.jp.

Here, we report the case of a Japanese girl with KID syndrome. The mutation analysis of GJB2 (the coding region of Cx26 gene) revealed a novel missense mutation, N14Y. This mutation is in the N-terminal domain of Cx26 where other mutations in KID syndrome have previously been reported; therefore, it is assumed that the N-terminal domain of Cx26 should be necessary for the proper function of the protein. To understand the function of this domain, it was important to clarify the relation between the N14Y mutation and the altered channel function of the gap junction. For this, we performed the following experiments: 1) ultrastructural examination of gap junctions and immunohistological study for Cx26 expression in the patient's skin was performed; 2) we investigated the effect of N14Y mutation on gap junctional intercellular communication by a dye transfer assay; and 3) we studied the structural changes in the N-terminal domain of Cx26 by molecular structural analysis using nuclear magnetic resonance (NMR).

Materials and Methods

Skin Samples and DNA

Skin biopsies were taken from the skin lesion on the left foot of the patient after informed consent. Genomic DNA samples from peripheral blood were obtained from the family members including the patient and her parents after informed consent.

Mutation Analysis

Genomic DNA was extracted from peripheral blood and used as a template of gene amplification. The coding region of GJB2 (GenBank accession no. NM 004004) was amplified by polymerase chain reaction (PCR), as previously described.[5] DNA sequencing of the PCR product was performed with an ABI Prism 3100-Avant genetic analyzer (Perkin Elmer-ABI, Foster City, CA).

Electron Microscopy

The skin sample was fixed in one-half strength Karnovsky's fixative or 2% glutaraldehyde solution, postfixed in 1% OsO_4, dehydrated, and embedded in Epon 812. The sample was ultrathin-sectioned at a thickness of 70 nm and stained with uranyl acetate and lead citrate. Photographs were taken using a Hitachi H-7100 transmission electron microscope (Hitachi High-Technologies Corporation, Tokyo, Japan).

Immunofluorescence Labeling

The patient's skin sample was snap-frozen in isopentane, and 6-μm-thick sections were cut using a cryostat. The sections were washed with 0.01 mol/L phosphate-buffered saline (PBS) for 10 minutes and then incubated in rabbit polyclonal anti-Cx26 antibody—the epitope is a portion of the cytoplasmic loop of Cx26—(Zymed Laboratories, San Francisco, CA) or mouse monoclonal anti-Cx43 antibody (clone 4E6.2; Chemicon International, Temecula, CA) solution for 1 hour at 37°C. Antibody dilutions were 1/10 for Cx26 antibody and 1/200 for Cx43 antibody. The sections were then incubated with fluorescein isothiocyanate-conjugated goat anti-rabbit immunoglobulins for Cx26 and fluorescein isothiocyanate-conjugated goat anti-mouse immunoglobulins for Cx43 (Jackson Immunoresearch Laboratories, West Grove, PA) solution for 30 minutes at room temperature, followed by 10 μg/ml propidium iodide solution as a nuclear counterstain (Sigma Chemical Co., St. Louis, MO) for 10 minutes. The sections were extensively washed with 0.01 mol/L PBS between incubations. The stained sections were mounted using a glycerol-based mounting medium (Permafluor, Shandon, PA) and stored in the refrigerator in the dark. Immunostaining was detected as green (fluorescein isothiocyanate), and nuclear staining was observed as red (propidium iodide). Overlap of both fluorescein isothiocyanate and propidium iodide was demonstrated as yellowish color. Fluorescence images were observed using an Olympus IX70 confocal laser-scanning microscope. Image collection was performed by software Fluoview version 2.0 (Olympus America Inc., Melville, NY).

Cell Culture

Cell culture was performed with slight modifications to the methods previously described.[6] A biopsy was taken from a hyperkeratotic plaque on the dorsum of the patient's left foot. Biopsy samples were kept in ice-cold PBS containing antibiotics (100 U/ml penicillin, 100 μg/ml streptomycin, 50 μg/ml gentamicin, 2.5 μg/ml amphotericin B, and 0.4% neomycin). After trimming subepidermal connective tissue, the samples were placed (overnight, 4°C) in dispase in PBS. The epidermis was peeled off from the tissue and placed in trypsin-ethylenediaminetetraacetic acid solution (0.25% trypsin in 0.05% ethylenediaminetetraacetic acid). Single cells were suspended in keratinocyte seeding medium.[7] Cells were seeded on mitomycin C-treated feeder layer of 3T3 cells in 35-mm-diameter tissue culture plates. Cultures were fed with Dulbecco's modified Eagle's medium, incubated at 37°C, 5% CO_2.

Dye Transfer Assay

The dye transfer assay was performed by scrape-loading methods introduced by el-Fouly and colleagues[8] with slight modification. Briefly, epidermal keratinocytes from the patient, normal human epidermal keratinocyte (NHEK), and HaCaT cells (human keratinocyte cell line) were grown to confluency on 35-mm plastic plates in Dulbecco's modified Eagle's medium. After removal of medium, the cells were scraped using a plastic eraser, and 0.125% Lucifer yellow and 0.05% rhodamine dextran (Molecular Probes, Eugene, OR) dissolved in PBS were immediately added to the cells. Two minutes later, the dye solution was discarded, and the plates were rinsed with adequate amounts of PBS to remove detached cells

and background fluorescence. Cells were examined under an Olympus IX70 confocal laser-scanning microscope (Olympus America Inc., Melville, NY) at the time of 20 minutes after scrape loading. The degree of dye transfer was quantified by counting the Lucifer yellow-positive cells per unit length (50 μm) of scratched plane. We counted only the Lucifer yellow-positive cells, and the cells that were both Lucifer yellow- and rhodamine-positive were excluded. The gap junction-mediated dye transfer was confirmed by the presence of red staining of rhodamine dextran at the edge of the scratched plane, because rhodamine dextran is 10 kd and cannot pass through the gap junction. Lucifer yellow, on the other hand, is 0.5 kd and can be transferred to other cells through gap junctions; therefore, it diffuses from the edge of the scratched plane to inner intact cells. Statistical analysis was performed using Student's *t*-test.

Peptide Synthesis

Wild-type and mutant peptides containing the 20 N-terminal amino acids of Cx26 (MDWGTLQTILGGVNKHSTSI and MDWGTLQTILGGVYKHSTSI, respectively) were synthesized by Sigma Genosys (Japan).

NMR Spectroscopy

The peptides were dissolved to a final concentration of 2 mmol/L in 350 μl of 90% H_2O/10% D_2O or 99.9% D_2O at pH 4.0. The pH was adjusted by adding μl increments of HCl and NaOH. The NMR experiments were performed on JEOL ECA 600 or Bruker DMX 500 spectrometers. The NMR spectra, DQF-COSY,[9] TOCSY,[10] and NOESY[11] were recorded at 10°C, and some experiments were also recorded at 20 and 30°C to resolve ambiguities. TOCSY spectra with a MLEV-17 sequence were collected with spin-lock times of 90 ms, and NOESY spectra were obtained with mixing times of 100 to 300 ms. The chemical shifts were measured from the internal standard of sodium 2,2-dimethyl-2-silapentane-5-sulfate. All two-dimensional spectra were processed using NMRPipe software.[12]

Circular Dichroism (CD) Measurement

All measurements were performed on a Jasco J-725 spectropolarimeter (Tokyo, Jasco, Japan). Sample solutions were buffered with 10 mmol/L potassium phosphate buffer (pH 7.0) in various 2,2,2-trifluoroethanol (TFE) concentrations. Spectra were recorded at 25°C and at peptide concentrations of 0.2 mmol/L using a quartz cell with a path length of 1 mm. All of the spectra were baseline-corrected by subtracting buffer spectra.

Results

Patient

The patient was a 4-year-old Japanese girl with no family history of skin disorders or auditory dysfunction. From birth, impetiginous erythema had been observed on her neck, axilla, and perianal areas. At the age of 4 months, spiky white keratotic papules appeared on her palms and soles, and impetiginous plaques were also noted on her occipital area. At the age of 2 years, she was referred to the otolaryngological clinic, and profound sensorineural deafness was noted. At the age of 4 years, keratitis was found on both eyes. She was diagnosed with KID syndrome at this time. By the age of 4 years, hyperkeratotic plaques were scattered on her scalp and extremities (Figure 1A). Palms and soles were severely hyperkeratotic (Figure 1, B and C).

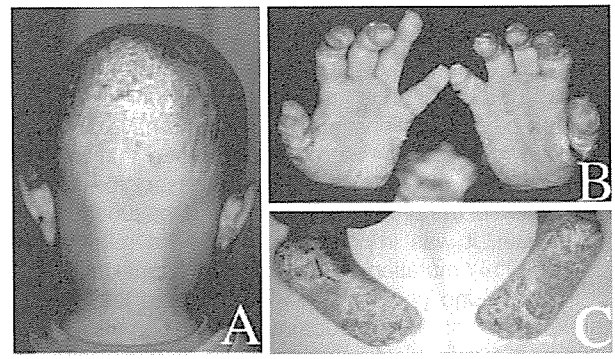

Figure 1. Clinical figures of the patient at the age of 4. **A:** Hyperkeratotic plaques on her scalp. She wears a hearing aid on the left side because of sensorineural deafness. **B** and **C:** Hyperkeratosis of her palms and soles.

Mutation Analysis

Direct sequencing of the patient's genomic DNA, amplified by PCR, revealed that the patient was heterozygous for a novel missense mutation NM_004004:c.40A>C resulting in the amino acid substitution asparagine to tyrosine (N14Y). This mutation results in the gain of a recognition site for the restriction enzyme Bsp1470I (Figure 2). N14Y was not found in her parents (Figure 2) and was

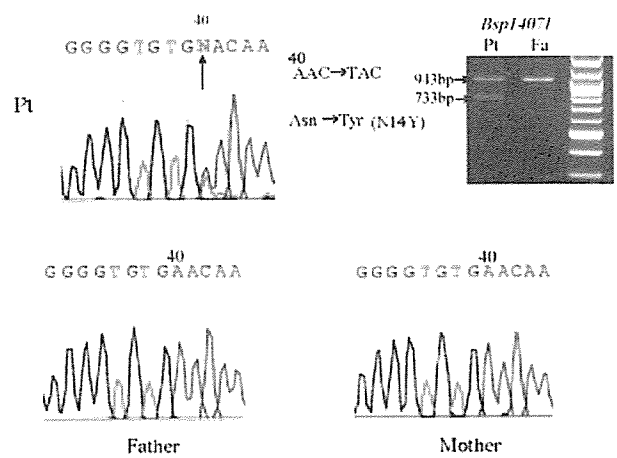

Figure 2. DNA sequences of GJB2. A heterozygous A to T transition at codon 40 is detected in the patient's gene (NM_004004:c.40A>T). This mutation leads to the amino acid substitution N14Y. This missense mutation is *de novo* because it is not found in the parent's DNA. N14Y results in the gain of a Bsp1407I restriction site. PCR products from the patient (Pt) are digested into fragments of 733 and 943 bp. In contrast, the digested PCR products from the father (Fa) show only the 943-bp band.

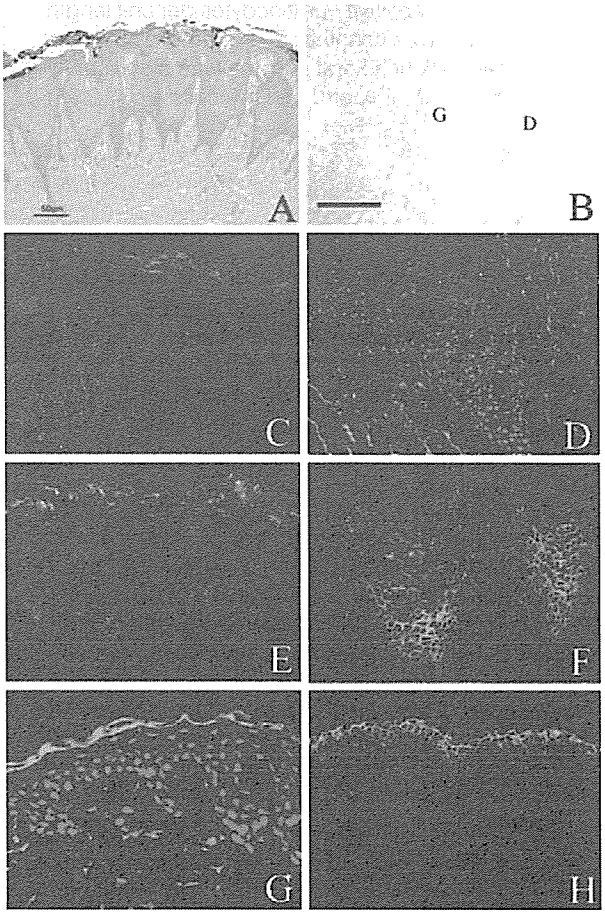

Figure 3. Skin morphology and immunofluorescence study. **A:** H&E staining. Hyperkeratosis with focal parakeratosis and regular acanthosis with broad rete ridges are observed. Granular layer was lost and vacuolar change of cytoplasm was seen in the upper spinous layer. **B:** Electron microscopy in the patient's skin (granular layer of the epidermis). The gap junctions have a typical pentalaminar structure, 20 nm in width. Abnormal junctional structures were not found. **D:** Desmosome, **G:** gap junction. **C–F:** Cx26 and Cx43 expression of the patient's epidermis. Green (fluorescein isothiocyanate) indicates Cx26 expression. Red (propidium iodide) is nuclear staining. **C:** Cx26 was expressed in the keratinocytes in the widened rete ridge. **D:** The staining of the Cx26 in the keratinocytes was more cytoplasmic than membranous, although punctate membranous staining was also seen in the acrosyringium cells. Cx43 expression was observed in the keratinocytes in the middle and upper epidermal layers (**E**) and was mostly membranous (**F**). **G:** Cx26 staining in normal skin. There was no expression of Cx26 in the normal epidermis. The staining at the corneum seemed to be nonspecific. **H:** Cx43 staining in normal skin. The staining was observed at the membrane of epidermal keratinocytes. Scale bar = 100 nm.

thought to be a *de novo* mutation. In addition, this mutation was not found in 50 normal unrelated Japanese alleles (25 normal unrelated Japanese individuals) and was unlikely to be a polymorphism. Direct sequencing of the entire coding region and borders of GJB2 failed to detect any other pathogenic mutation in the patient's DNA.

Skin Morphology

Skin biopsy obtained from the lesional skin revealed hyperkeratosis with focal parakeratosis and regular acanthosis with broad rete ridges (Figure 3A). Granular layer was absent, and vacuolar change of cytoplasm was observed in the upper spinous layer. Electron microscopy demonstrated gap junctions in all epidermal layers, with normal morphology showing typical pentalaminar structures 20 nm in width (Figure 3B). Immunofluorescence showed Cx26 expression in the upper layer of wide rete ridge in the patient's epidermis (Figure 3C), compared with the normal epidermis that does not express Cx26 (Figure 3G). The staining of Cx26 was more cytoplasmic than membranous in the keratinocytes of the upper layer, although punctate staining on cellular interface was also observed in the acrosyringium cells (Figure 3D). We also examined Cx43 expression in the patient's epidermis because Cx43 is the major Cx expressed in the epidermis. Cx43 staining was seen in the middle and upper epidermal layer, similar to the expression of Cx26 in the patient's skin (Figure 3E). The expression of Cx43 was almost completely membranous (Figure 3F) and seemed to be the same as in normal control skin (Figure 3H). The antibody used in the present study binds to both normal and mutant Cx26 peptides; thus, it was not clear whether the overexpressed Cx26 in the patient's epidermis was normal and/or mutated.

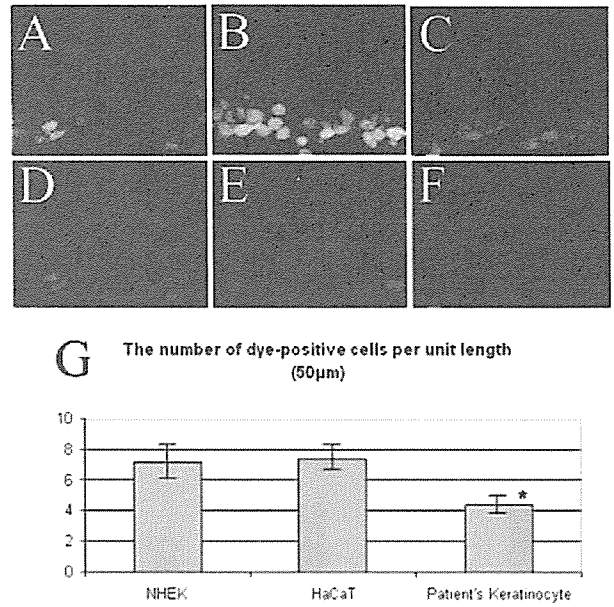

Figure 4. Dye transfer assay of cultured keratinocyte. **A:** NHEK. **B:** HaCaT. **C:** Keratinocytes of KID syndrome. The diffusion of Lucifer yellow of patient's keratinocytes was less than in NHEK and HaCaT cells. Rhodamine dextran (red) is observed at the edge of the scratched plane because the rhodamine dextran molecule is too bulky to pass through gap junctions (**D–F:** NHEK, HaCaT, and patient's keratinocyte, respectively). **G:** The number of Lucifer yellow-positive cells per unit length of scratched plane. The number of positive cells of the patient's keratinocytes was significantly smaller than that of NHEK and HaCaT. NHEK: 7.17 ± 1.14 (average ± SD); HaCaT: 7.43 ± 1.07; patient's cell: 4.34 ± 0.75. $^*P < 0.01$ by Student's *t*-test.

Dye Transfer

The transfer of dye between cells was observed in all cell types, although the degree of dye transfer of cultured patient's keratinocytes was less than in NHEK and HaCaT cells, indicating abnormality of gap junctional intercellular communication in the patient (Figure 4, A–C). The num-

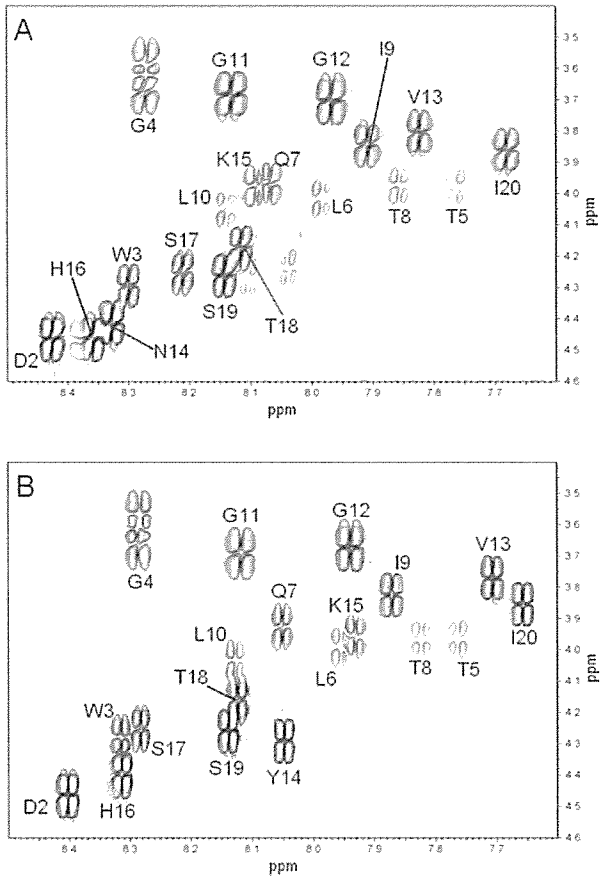

Figure 5. Comparison of the fingerprint region from DQF-COSY spectra of wild type (**A**) and N14Y mutant (**B**). The mutation does not cause significant change in chemical shifts when compared to wild type.

ber of Lucifer yellow-positive keratinocytes per unit length of scratched plane was counted. The number of positive cells in cultured patient's keratinocytes was significantly smaller than that in NHEK and HaCaT cells ($P < 0.01$) (Figure 4G).

NMR Analysis

The chemical shift assignments of wild-type and mutant peptides were performed according to standard procedure of sequential assignment.[13] An almost complete assignment of the proton NMR signals of wild-type and mutant peptides was obtained. A comparison between the DQF-COSY spectra of the fingerprint regions of wild type and mutant, with the results of assignment, is shown in Figure 5.

To compare clearly the structural properties of these two peptides, chemical shift differences of α-protons and amide protons are plotted in Figure 6. Figure 6A shows that the patterns of chemical shift deviation of the mutant peptide from random coil structure resemble that of wild-type peptide in both CαH and NH. In addition, continuous negative values of chemical shift deviations of CαH in the N-terminal region (Trp3-Leu10) suggest formation of helical conformation in both wild type and mutant. Thus, the three-dimensional structural properties of these two peptides are thought to be basically the same. This result is further confirmed by the data that large changes in shift between wild type and mutant are only observed for resonances around the mutated residue N14Y (Figure 6B). It is reasonable to think that the conformation of mutant peptide maintains its wild-type form because the chemical shifts of α-protons and amide protons are very sensitive to backbone conformation and secondary structure.

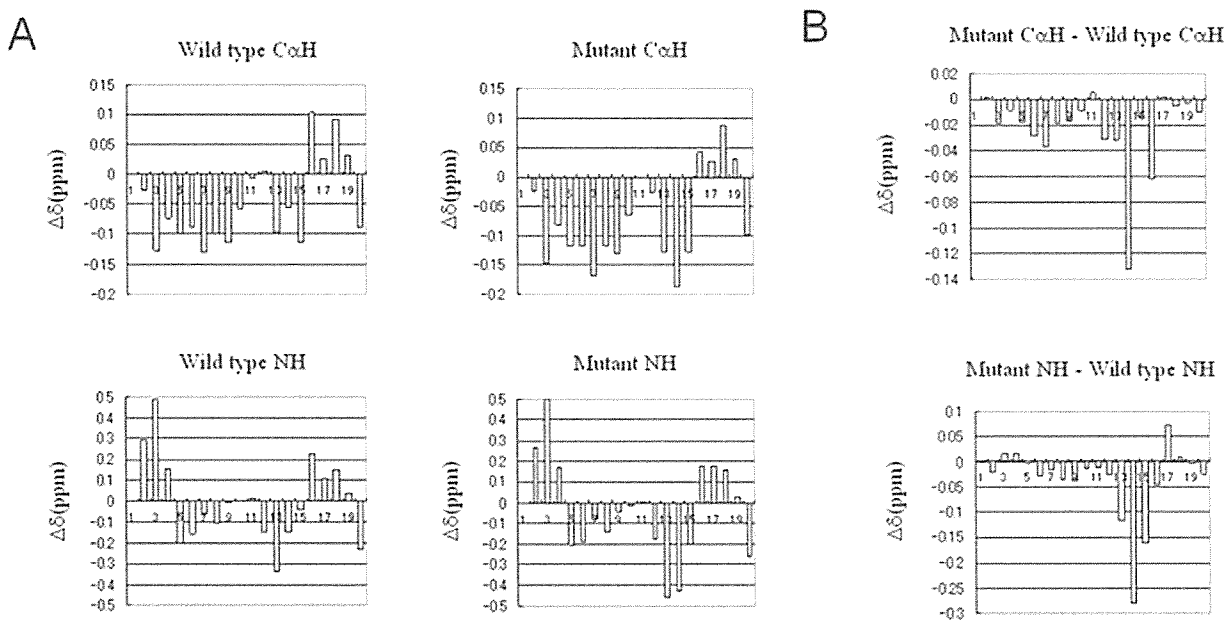

Figure 6. Chemical shift differences of amino acid residues in wild type and N14Y mutant. **A:** The differences in chemical shift defined as δ (wild-type or mutant peptide)-δ (random coil) are plotted. **B:** The differences in chemical shift defined as wild-type peptide-mutant are plotted.

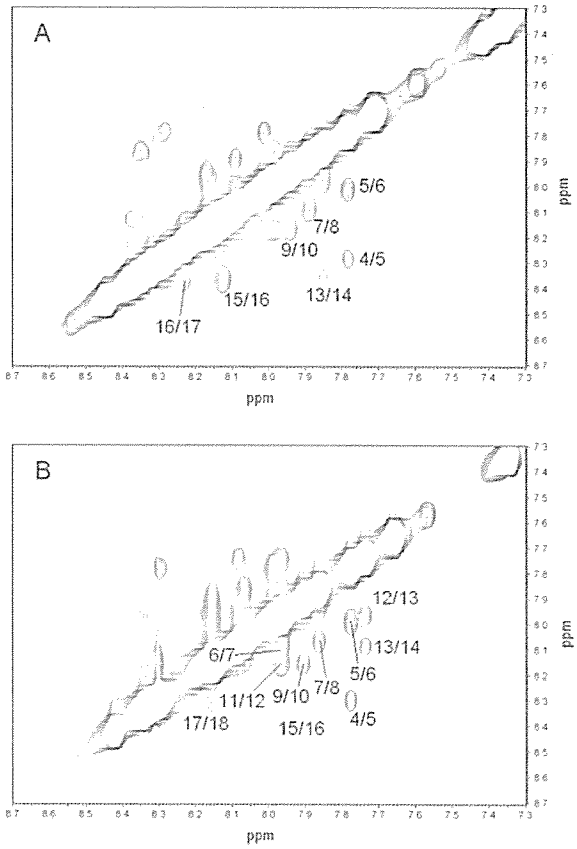

Figure 7. NH-NH regions from NOESY spectra of wild-type (**A**) and N14Y mutant (**B**) peptides. Sequential NH-NH cross-peaks are annotated.

Unfortunately, the number of NOEs (nuclear Overhauser effects) observed in our experiments was not sufficient for structural calculation. However, the NOE data did suggest the formation of an α-helical conformation, especially in the N-terminal region. Figure 7 shows the NH-NH region from NOESY spectra of wild-type and mutant peptide. In both spectra, a number of sequential NH-NH NOEs were observed and these results indicated that these peptides have propensity to adopt α helical structure. Although the basic NOE pattern of the mutant peptide agreed with that of wild-type one, some novel NOEs were observed from Tyr14 (Figure 8). In particular, a number of medium-range NOEs from the side chain of Tyr14, such as between δH of Tyr14 and αH of Gly12, εH of Tyr14. and αH of Gly 12, εH of Tyr14 and αH of His16 were observed. In contrast, no medium-range NOEs were observed in this C-terminal region in the case of wild-type peptide.

CD Measurement

The far-UV CD spectra were recorded for wild-type and mutant peptides derived from the N-terminal 20 amino acids of Cx26 (Figure 9). In water, the CD spectra of both wild-type and mutant peptides showed random-like conformational features (Figure 9A). The α-helix contents of these peptides are estimated to be considerably low judged from the value at 222 nm. On the other hand, in

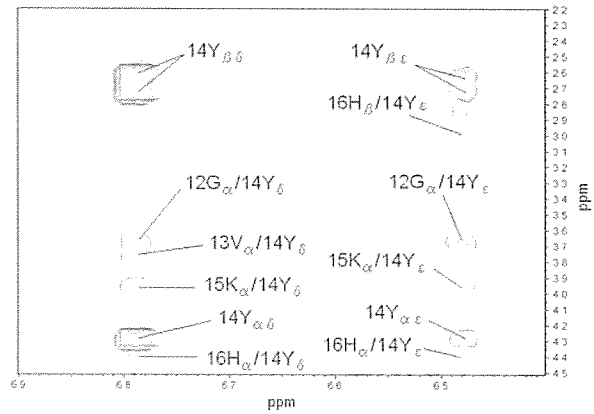

Figure 8. Novel NOE signals in N14Y mutant.

the case of CD spectra in TFE solution, the α-helical contents increased with increasing TFE concentration (Figure 9B). Although the conformational changes were induced by TFE in both wild-type and mutant peptides, α-helical structure was induced more easily and strongly in the case of mutant one.

Discussion

Eighty different types of Cx26 mutations have been reported in congenital deafness disorders (refer to the Cx-deafness homepage at *http://davinci.crg.es/deafness/*). Cx26-related nonsyndromic deafness is inherited in an autosomal dominant or recessive manner whereas Cx26-related syndromic deafness shows only an autosomal dominant inheritance trait. The reported mutations in syndromic Cx26-related deafness are summarized in Figure 10.[4,14–23] To date, five Cx26 mutations resulting in KID syndrome have been reported in the literature.[4,15,16] Among them, two mutations, G12R and S17F, exist in the N-terminal domain of Cx26, similar to our case (N14Y).

The asparagine (N) at position 14 is highly conserved across the species and also across Cx families (GJB1 to 6), supporting the pathogenicity of this mutation.[14] In addition, this mutation was not found in the normal control samples in this study, nor was it detected in another report that checked 192 control Japanese alleles.[24] N14K mutation in Cx26 was reported recently in a patient with Clouston syndrome-like phenotype with deafness.[14] In this report the position of the mutated amino acid is identical to that of our study; however, the resultant clinical phenotype differs markedly from our patient. This patient had congenital sensorineural deafness but no keratitis, and the skin showed only mild erythrokeratoderma, mild hypotrichosis, and brittle nails. These clinical differences indicate that the chemical property of altered amino acid may be crucial for the phenotype in addition to the position of the mutation. Tyrosine (Y) has a benzene ring, and lysine (K) has an amino residue; thus the difference of the chemical characters of altered amino acid may influence Cx assembly and gap junction channel selectivity because of their molecular sizes, electronic charges, and hydrophilicity. It is interesting that another

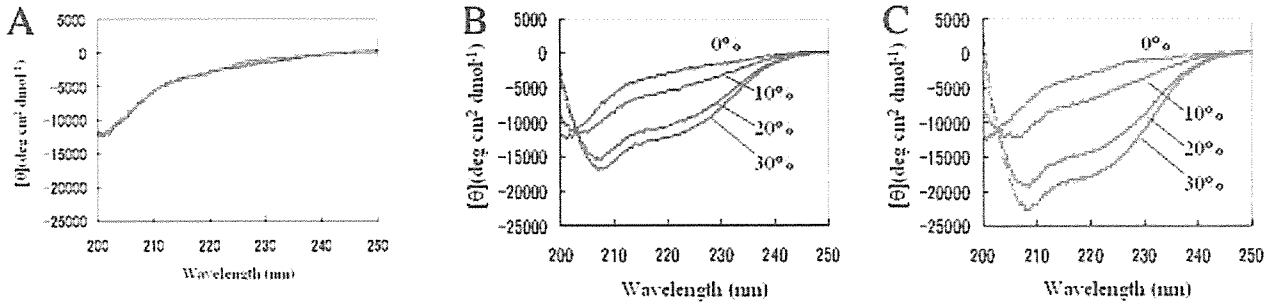

Figure 9. Far-UV CD spectra of wild-type and mutant peptides. Wild-type (blue) and mutant peptide (red) were measured in water (**A**) and in various TFE concentrations (**B**, **C**). The numbers indicate the percentage of TFE.

mutation in the N terminus of Cx26 in KID syndrome, S17F (serine to phenylalanine), is similar to the N14Y mutation in that both mutations result in the replacement of a hydrophilic amino acid to one with a benzene ring.

Despite the mutation of Cx26 in our patient, the morphology of gap junctions observed by electron microscopy seemed to be normal, and disturbed adhesional structures were not observed in the specimens. In a report of erythrokeratoderma variabilis with Cx31 mutation, morphological changes of gap junctions were also not observed.[25] In our case, the mutation was in the cytoplasmic side; therefore, the coupling of connexons with those of opposite cells at the extracellular site might not be affected, resulting in normal morphology of gap junctions. Otherwise, the normal gap junction structures seen in the patient's skin sample may consist of Cx43, which was expressed normally in the patient's skin.

By immunofluorescence study, the expression of Cx26 was observed in the upper layer of the epidermis in our patient. In normal skin, Cx26 expression is not seen in the epidermis, although strong expression is observed in the hair follicle and the sweat duct and gland.[26] However, in some of the hyperkeratotic skin disorders such as psoriasis, Cx26 expression is seen in the upper layer of the epidermis.[27] Cx26 expression in the epidermis of patients with KID syndrome has also been previously reported.[4] The Cx26 staining in the epidermis of our patient confirmed *in vivo* expression of Cx26 in the patient's keratinocytes and supported the pathological significance of this protein for the hyperkeratotic changes of the epidermis.

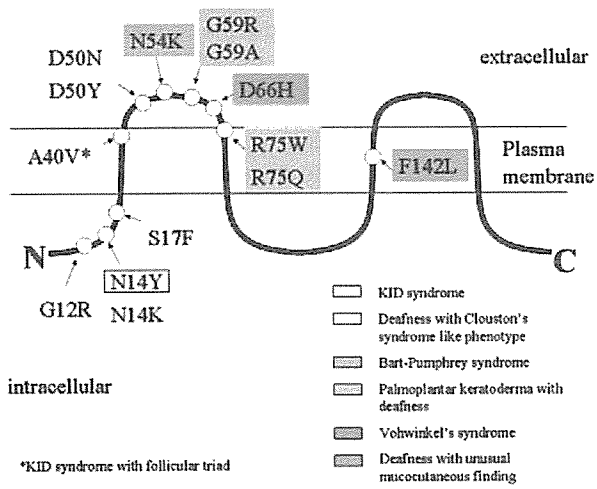

Figure 10. The Cx26 mutations of syndromic sensorineural deafness reported in the literature. The mutations of KID syndrome are aggregated to the N-terminal side of Cx26, especially in the cytoplasmic portion.

The transfer of dye between cells was reduced in the patient's keratinocytes compared to NHEK and HaCaT cells. This result directly proved that the channel function of gap junctions was affected by the Cx26 mutation, N14Y. The dye transfer was not completely impaired in the patient's keratinocytes, probably because other Cx molecules, such as Cx43, can work partly independently of mutated Cx26. However, certain Cx26 mutations were reported to dominantly inhibit normal Cx43 function, demonstrated by coupling transfection of the mRNA of wild-type and mutant Cxs into *Xenopus* oocytes.[28] Therefore, a part of impairment of gap junctional intercellular communication may be because of trans-dominant inhibition of mutated Cx26 to functions of other intact Cxs.

Our NMR data of N-terminal peptides of human Cx26 in water suggested that both wild-type and mutated peptides have basically the same conformational feature. The chemical shift differences of CαH between the experimental shifts for the peptides and random coil shifts (Figure 6) clearly suggested that these peptides have a tendency to form α-helical structures, except for a few residues in the C termini. In addition, NOE data also showed formation of α-helix-like conformation in some N-terminal residues. However, the number of NOEs observed in our studies was not sufficient to confirm that these peptides form rigid α-helical conformation in water. In addition, CD data also suggested that helical contents of these peptides were low in water although α-helical structures were induced by considerably low TFE concentrations. Thus, these peptides are likely to have relatively high flexibility in water even though rigid helical structures are easily induced by nonpolar environments, such as in TFE solvent. In water, there were no significant differences between CD spectra of these peptides. However, the secondary structure of mutant peptide is susceptible to induction of TFE. Thus, the mutation may change the conformational flexibility of the peptide and the helical propensity.

Recently, sequence-specific ^{1}H NMR resonance assignment for the N-terminal 15-amino acid peptide derived from rat Cx26 have been reported.[29] The primary structures of the N-terminal domain of Cx26 are highly

conserved in mammals, and the difference between human and rat is only one residue (Thr8 in human to Ser8 in rat) in this N-terminal region. Our peptides synthesized from human Cx26 sequence are slightly longer than the peptide derived from rat (15 residues long). The results of NMR studies from rat Cx26 showed that the peptide has a more highly ordered structure than our human Cx26 peptide although the conformational features of rat Cx26 peptides basically agree with our human one. These peptides are highly homologous except in their length. Thus, the difference in flexibly may be attributable to the extension of C-terminal residues. Previous analysis of the rat Cx26 peptide suggested the importance of flexibility in the hinge region (Gly12 and Gly13) in the placement of the N-terminal residues within the channel pore. In the present study, some NOEs to these glycine residues, which were not observed in the wild-type peptide, appeared in the N14Y mutant. Thus, it is likely that the N14Y mutation induced a change in local flexibility and that the motion of the N-terminal residues, which are important for the channel function of the protein, was altered profoundly.

References

1. Kelsell DP, Dunlop J, Hodgins MB: Human diseases: clues to cracking the connexin code? Trends Cell Biol 2001, 11:2–6
2. Rabionet R, Lopez-Bigas N, Arbones ML, Estivill X: Connexin mutations in hearing loss, dermatological and neurological disorders. Trends Mol Med 2002, 8:205–212
3. Maestrini E, Korge BP, Ocana-Sierra J, Calzolari E, Cambiaghi S, Scudder PM, Hovnanian A, Monaco AP, Munro CS: A missense mutation in connexin26, D66H, causes mutilating keratoderma with sensorineural deafness (Vohwinkel's syndrome) in three unrelated families. Hum Mol Genet 1999, 8:1237–1243
4. Richard G, Rouan F, Willoughby CE, Brown N, Chung P, Ryynanen M, Jabs EW, Bale SJ, DiGiovanna JJ, Uitto J, Russell L: Missense mutations in GJB2 encoding connexin-26 cause the ectodermal dysplasia keratitis-ichthyosis-deafness syndrome. Am J Hum Genet 2002, 70:1341–1348
5. Richard G, White TW, Smith LE, Bailey RA, Compton JG, Paul DL, Bale SJ: Functional defects of Cx26 resulting from a heterozygous missense mutation in a family with dominant deaf-mutism and palmoplantar keratoderma. Hum Genet 1998, 103:393–399
6. Grossman N, Slovik Y, Bodner L: Effect of donor age on cultivation of human oral mucosal keratinocytes. Arch Gerontol Geriatr 2004, 38:114–122
7. Rheinwald J: Cell Growth and Division: A Practical Approach. Edited by Baserga R. Oxford, IRL Press, 1989, pp 81–94
8. el-Fouly MH, Trosko JE, Chang CC: Scrape-loading and dye transfer. A rapid and simple technique to study gap junctional intercellular communication. Exp Cell Res 1987, 168:422–430
9. Rance M, Sørensen OW, Bodenhausen G, Wagner G, Ernst RR, Wüthrich K: Improved spectral resolution in cosy 1H NMR spectra of proteins via double quantum filtering. Biochem Biophys Res Commun 1983, 117:479–485
10. Braunschweiler L, Ernst RR: Coherence transfer by isotropic mixing: application to proton correlation spectroscopy. J Magn Reson 1983, 53:521–528
11. Macura S, Huang Y, Suter D, Ernst RR: Two-dimensional chemical exchange and cross-relaxation spectroscopy of coupled nuclear spins. J Magn Reson 1981, 43:259–281
12. Delaglio F, Grzesiek S, Vuister GW, Zhu G, Pfeifer J, Bax A: NMRPipe: a multidimensional spectral processing system based on UNIX pipes. J Biomol NMR 1995 6:277–293
13. Wüthrich K: NMR of Proteins and Nucleic Acids. New York, John Wiley and Sons NY, 1986
14. van Steensel MA, Steijlen PM, Bladergroen RS, Hoefsloot EH, Ravenswaaij-Arts CM, van Geel M: A phenotype resembling the Clouston syndrome with deafness is associated with a novel missense GJB2 mutation. J Invest Dermatol 2004, 123:291–293
15. Montgomery JR, White TW, Martin BL, Turner ML, Holland SM: A novel connexin 26 gene mutation associated with features of the keratitis-ichthyosis-deafness syndrome and the follicular occlusion triad. J Am Acad Dermatol 2004, 51:377–382
16. Yotsumoto S, Hashiguchi T, Chen X, Ohtake N, Tomitaka A, Akamatsu H, Matsunaga K, Shiraishi S, Miura H, Adachi J, Kanzaki T: Novel mutations in GJB2 encoding connexin-26 in Japanese patients with keratitis-ichthyosis-deafness syndrome. Br J Dermatol 2003, 148:649–653
17. Richard G, Brown N, Ishida-Yamamoto A, Krol A: Expanding the phenotypic spectrum of Cx26 disorders: Bart-Pumphrey syndrome is caused by a novel missense mutation in GJB2. J Invest Dermatol 2004, 123:856–863
18. Heathcote K, Syrris P, Carter ND, Patton MA: A connexin 26 mutation causes a syndrome of sensorineural hearing loss and palmoplantar hyperkeratosis (MIM 148350). J Med Genet 2000, 37:50–51
19. Maestrini E, Korge BP, Ocana-Sierra J, Calzolari E, Cambiaghi S, Scudder PM, Hovnanian A, Monaco AP, Munro CS: A missense mutation in connexin26, D66H, causes mutilating keratoderma with sensorineural deafness (Vohwinkel's syndrome) in three unrelated families. Hum Mol Genet 1999, 8:1237–1243
20. Richard G, White TW, Smith LE, Bailey RA, Compton JG, Paul DL, Bale SJ: Functional defects of Cx26 resulting from a heterozygous missense mutation in a family with dominant deaf-mutism and palmoplantar keratoderma. Hum Genet 1998, 103:393–399
21. Uyguner O, Tukel T, Baykal C, Eris H, Emiroglu M, Hafiz G, Ghanbari A, Baserer N, Yuksel-Apak M, Wollnik B: The novel R75Q mutation in the GJB2 gene causes autosomal dominant hearing loss and palmoplantar keratoderma in a Turkish family. Clin Genet 2002, 62:306–309
22. Brown CW, Levy ML, Flaitz CM, Reid BS, Manolidis S, Hebert AA, Bender MM, Heilstedt HA, Plunkett KS, Fang P, Roa BB, Chung P, Tang HY, Richard G, Alford RL: A novel GJB2 (connexin 26) mutation, F142L, in a patient with unusual mucocutaneous findings and deafness. J Invest Dermatol 2003, 121:1221–1223
23. Leonard NJ, Krol AL, Bleoo S, Somerville MJ: Sensoryneural hearing loss, striate palmoplantar hyperkeratosis, and knuckle pads in a patient with a novel connexin 26 (GJB2) mutation. J Med Genet 2005, 42:e2
24. Abe S, Usami S, Shinkawa H, Kelley PM, Kimberling WJ: Prevalent connexin 26 gene (GJB2) mutations in Japanese. J Med Genet 2000, 37:41–43
25. Wilgoss A, Leigh IM, Barnes MR, Dopping-Hepenstal P, Eady RA, Walter JM, Kennedy CT, Kelsell DP: Identification of a novel mutation R42P in the gap junction protein beta-3 associated with autosomal dominant erythrokeratoderma variabilis. J Invest Dermatol 1999, 113:1119–1122
26. Salomon D, Masgrau E, Vischer S, Ullrich S, Dupont E, Sappino P, Saurat JH, Meda P: Topography of mammalian connexin in human skin. J Invest Dermatol 1994, 103:240–247
27. Labarthe MP, Bosco D, Saurat JH, Meda P, Salomon D: Upregulation of connexin 26 between keratinocytes of psoriatic lesions. J Invest Dermatol 1998, 111:72–76
28. Rouan F, White TW, Brown N, Taylor AM, Lucke TW, Paul DL, Munro CS, Uitto J, Hodgins MB, Richard G: Trans-dominant inhibition of connexin-43 by mutant connexin-26: implications for dominant connexin disorders affecting epidermal differentiation. J Cell Sci 2001, 114:2105–2113
29. Purnick PE, Benjamin DC, Verselis VK, Bargiello TA, Dowd TL: Structure of the amino terminus of a gap junction protein. Arch Biochem Biophys 2000, 381:181–190

Presence of Circulating CCR10+ T cells and Elevated Serum CTACK/CCL27 in the Early Stage of Mycosis Fungoides

Yasuyuki Fujita,[1] Riichiro Abe,[1] Mikako Sasaki,[1] Ayumi Honda,[1] Megumi Furuichi,[2] Yukie Asano,[2] Osamu Norisugi,[2] Tadamichi Shimizu,[2] and Hiroshi Shimizu[1]

Abstract

Purpose: Mycosis fungoides (MF), a common type of cutaneous T cell lymphoma with an indolent clinical course, has the characteristic that malignant T cell clones are recruited into the skin from the early disease stages. The mechanisms of recruitment have been suggested from our knowledge of various chemokine-chemokine receptor interactions. Recently, CCR10 and CTACK/CCL27 were proposed to play a role in the recruitment of other types of cutaneous T cell lymphoma. We examined the expression of CCR10 in peripheral blood and serum CTACK/CCL27 levels in patients with MF.

Experimental Design: Eighteen patients with MF, six patients with atopic dermatitis, and nine healthy volunteers were enrolled in our investigation. We investigated the differences in CCR10+ CD4+ expression in peripheral blood mononuclear cells by flow cytometry. Serum CTACK/CCL27 levels were determined using a CTACK/CCL27 ELISA assay kit.

Results: The number of circulating CCR10+ CD4+ cells was significantly higher in MF peripheral blood than in controls, even during the early stages. In lesional MF skin, infiltrating tumor cells also showed extensive expression of CCR10. The serum level of CTACK/CCL27 was higher in patients with MF than normal controls, but no statistical difference was found compared with atopic dermatitis patients.

Conclusions: CCR10-CTACK/CCL27 interactions between circulating T cells and keratinocytes would seem to play an important role in the pathophysiology of MF from the early disease stages.

Mycosis fungoides (MF) is the most common cutaneous T cell lymphoma (CTCL), with an estimated incidence of 0.5 cases per 100,000 population per year in the western world (1). MF has a classically slow clinical course that progresses over years through the patch, plaque, and tumor stages, followed by lymph nodes and visceral involvement (2). In MF, although malignant T cells persist mainly in skin and only few cells circulate in peripheral blood, recent studies have revealed an aberrant T cell immunophenotype and circulating clonal cutaneous lymphocyte antigen (CLA)-positive T cells in patients' blood (3–5). It was also shown that CLA+ CD4+ T cells express the CC chemokine receptor 4 (CCR4), which is suspected of playing a role in skin-homing. CCR4 was originally discovered in memory T cells (6, 7). Furthermore, Sokolowska-Wojdylo et al. reported that another CC chemokine receptor associated with skin-homing, CCR10, is expressed in circulating clonal CLA+ CD4+ cells in Sézary syndrome (8). Another study showed that malignant T cells expressing CCR10 were infiltrated in skin tissues in Sézary syndrome, MF, and unspecified CTCL (9).

Cutaneous T cell attracting chemokine (CTACK/CCL27) is a skin-associated chemokine that attracts skin-homing memory T cells (10). CTACK/CCL27 is known to be the ligand for CCR10, and is mainly produced by activated keratinocytes in various diseases such as atopic dermatitis, psoriasis, drug reactions, and other inflammatory conditions (11, 12). CTACK/CCL27 is also expressed by dermal components and by the microvasculature, playing an important role in recruiting T cells into skin (13).

We hypothesized that CCR10-CTACK/CCL27 interactions play an early role in the pathophysiology of MF from the patch stage. In this report, we have examined the expression of CCR10 in CD4+ cells circulating in patients without apparent MF peripheral blood involvement. In addition, we have determined the concentration of CTACK/CCL27 protein contained in MF patients' serum.

Materials and Methods

Materials. The following monoclonal antibody was used in this study: CD4 was from BD Bioscience (San Jose, CA), CCR10 from Immuno Detect, Inc. (Fayetteville, NY), CTACK/CCL27 from R&D systems (Minneapolis, MN). DMEM was purchased from Invitrogen (Groningen, Netherlands), collagenase from Wako Pure Chemical (Osaka, Japan), Ficoll from Amersham Biosciences Corp. (Piscataway, NJ), human CTACK/CCL27 ELISA assay kit was from R&D Systems. All other chemicals were of reagent grade or higher.

Authors' Affiliations: [1]Department of Dermatology, Hokkaido University Graduate School of Medicine, Sapporo, and [2]Department of Dermatology, Faculty of Medicine, University of Toyama, Toyama, Japan

Received 7/12/05; revised 12/27/05; accepted 2/8/06.

The costs of publication of this article were defrayed in part by the payment of page charges. This article must therefore be hereby marked *advertisement* in accordance with 18 U.S.C. Section 1734 solely to indicate this fact.

Requests for reprints: Yasuyuki Fujita, Department of Dermatology, Hokkaido University Graduate School of Medicine, Sapporo 060-8638, Japan. Phone: 81-11-716-1161, ext. 5962; Fax: 81-11-706-7820; E-mail: yfujita@med.hokudai.ac.jp.

doi:10.1158/1078-0432.CCR-05-1513

Table 1. Clinical characteristics of patients with MF

Patient no.	Age, sex	Duration (mo)	Clinical stage	Tumor-node-metastasis-blood classification, stage	sIL-2R (units/mL)	LDH (IU/L)	CCR10 in PBMC (%)	Serum CTACK/CCL27 (pg/mL)
1	72, M	31	Patch	$T_1N_0M_0B_0$, stage IA	243	154	0.55	600
2	66, M	430	Patch	$T_1N_0M_0B_0$, stage IA	372	194	5.19	630
3	36, F	240	Patch	$T_{2a}N_0M_0B_0$, stage IB	549	153	3.02	760
4	41, F	168	Patch	$T_{2a}N_0M_0B_0$, stage IB	262	151	1.29	660
5	67, M	35	Patch	$T_1N_0M_0B_0$, stage IA	357	200	3.36	620
6	67, M	10	Plaque	$T_{2b}N_0M_0B_0$, stage IIB	1,273	273	2.99	1,560
7	68, F	580	Plaque	$T_{2b}N_0M_0B_0$, stage IIB	796	191	0.96	910
8	50, M	9	Plaque	$T_{2b}N_0M_0B_0$, stage IIB	408	195	1.76	1,510
9	52, F	24	Plaque	$T_{2b}N_0M_0B_0$, stage IIB	425	192	4.58	1,650
10	87, F	270	Plaque	$T_{2b}N_3M_0B_0$, stage IVA	658	220	1.52	1,320
11	37, F	184	Plaque	$T_{2b}N_1M_0B_0$, stage IIB	<198	198	0.38	920
12	61, M	170	Plaque	$T_{2b}N_0M_0B_0$, stage IIB	399	154	1.08	920
13	60, F	75	Plaque	$T_{2b}N_0M_0B_0$, stage IIB	253	146	0.78	1,040
14	82, F	240	Plaque	$T_{2b}N_0M_0B_0$, stage IIB	223	173	2.33	760
15	80, F	128	Plaque	$T_{2a}N_0M_0B_0$, stage IB	1,301	201	0.45	680
16	49, M	26	Tumor	$T_3N_0M_0B_0$, stage IIIA	554	146	3.39	1,010
17	68, M	82	Tumor	$T_3N_0M_0B_0$, stage IIIA	813	202	5.3	1,500
18	60, F	106	Tumor	$T_3N_0M_0B_0$, stage IIIA	1,200	188	0.64	850

Patients and controls. Eighteen patients with MF (eight men and 10 women: mean age, 61.3 years old) from the Department of Dermatology at Hokkaido University Graduate School of Medicine were enrolled in this study (Table 1; Fig. 1). MF was diagnosed on the basis of clinical images, histopathologic findings from skin biopsies (all cases), and gene rearrangement analysis from skin tissue. Clinical stages were also evaluated according to the modified staging classification for CTCL proposed by Kashani-Sabet et al. (14). The evaluations of clinical images, including the clinical stages, were done by a single qualified dermatologist. Blood and serum samples were collected under proper, informed consent. In two patients at the tumor stage, tumor samples were analyzed for flow cytometry analysis. For control purposes, nine healthy volunteers and six atopic dermatitis patients who had widespread skin lesions with moderate activity were also investigated.

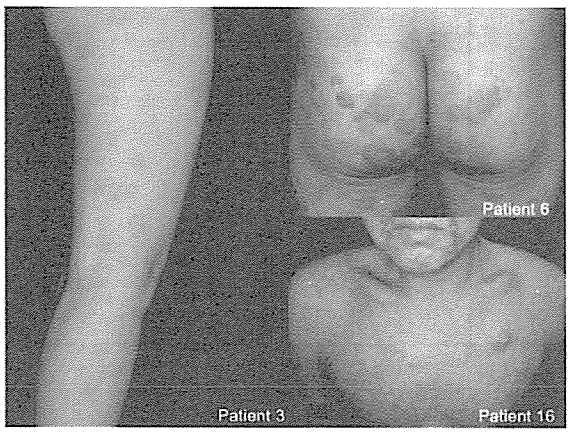

Fig. 1. Clinical images. *Patient 3,* pink-red maculae disseminated on the legs (patch stage). *Patient 6,* infiltrated erythematous plaques on the buttocks (plaque stage). *Patient 16,* poikilodermatous erythema, plaques and ulcerated nodules (tumor stage).

Flow cytometry. Peripheral blood mononuclear cells (PBMC) were isolated from heparinized venous blood by density gradient centrifugation using Ficoll. Two-color flow cytometry was done by incubation of cells (2×10^6) at 4°C. Staining for CCR10 done with monoclonal antibody against CCR10 followed by PE-labeled goat anti-mouse IgG (Rockland Immunochemical, Gilbertsville, PA) and FITC-conjugated antihuman CD4 monoclonal antibody (BD PharMingen, San Diego, CA). Cells were analyzed using a FACScan flow cytometer (Becton Dickinson, San Jose, CA), and CellQuest software (Becton Dickinson). Tumor cells were obtained from two patients' biopsy materials. The biopsy material was incubated with 200 units/mL collagenase in DMEM with 5% FCS at 37°C for 30 minutes. Suspensions were washed twice with PBS, and 50-μm filters were used to remove larger tissue fragments. Cells (1×10^6) were prepared for two-color analysis by resuspending in PBS containing 1% FCS and 1% bovine serum albumin, and flow cytometry was done as described above.

ELISA. Serum CTACK/CCL27 levels were determined using a CTACK/CCL27 ELISA kit assay in patients with MF, patients with atopic dermatitis, and healthy volunteers. We used a 96-well polystyrene microplate coated with a murine monoclonal antibody against human CTACK/CCL27. Optical densities were measured at 450 nm with a Bio-Rad Model 550 microplate reader (Bio-Rad Laboratories, Inc., Hercules, CA). The protein levels were calculated from a standard curve generated by a curve-fitting program.

Immunohistochemistry. Paraffin-embedded skin tissues from patients with MF were cut into 4-μm-thick sections. To prepare the sections for immunohistochemical analysis, they were pretreated with 3% hydrogen peroxide for 10 minutes at 4°C. They were stained with avidin-biotin peroxidase complex procedure using a Vector ABC Kit (Vector Laboratories, Burlingame, CA) according to the manufacturer's protocol. In brief, samples were treated with 10% normal goat serum for 30 minutes at room temperature followed by overnight incubation with the anti-CTACK/CCL27 monoclonal antibody or anti-CCR10 monoclonal antibody at 4°C. Positive staining was visualized with diaminobenzidine as a chromogen using a streptavidin-biotin peroxidase.

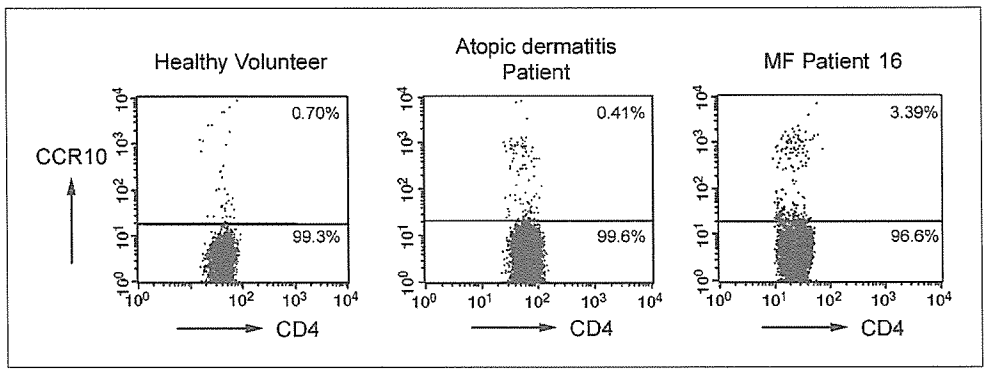

Fig. 2. PBMC CCR10 expression. PBMCs were stained with the indicated monoclonal antibodies and analyzed by flow cytometry (*left,* healthy volunteer; *middle,* atopic dermatitis patient; *right,* MF patient). The MF patient expressed more CCR10+ in circulating T cells.

Statistics. Differences between various treatments were statistically tested using Mann-Whitney *U* tests. $P < 0.05$ was considered statistically significant. Data in the figures are shown as the mean ± SE of multiple samples.

Results

Flow cytometric analysis of CCR10 expression in circulating CD4+ cells. Representative flow cytometry analyses of the surface expressions of CD4 and CCR10 in a healthy volunteer, an atopic dermatitis patient, and MF patient 16 are shown in Fig. 2. Summary of percentages of CCR10+ CD4+ cells in the CD4+ T cell population is shown in Fig. 3. The average percentages of CCR10+ cells were 0.91 ± 0.13%, 0.55 ± 0.15%, and 2.19 ± 0.39% in healthy volunteers ($n = 9$), patients with atopic dermatitis ($n = 6$) and patients with MF ($n = 18$), respectively. Patients with MF express significantly more CCR10+ CD4+ cells ($P < 0.05$). When classified into clinical stages of MF, the average percentages were 2.68 ± 0.82%, 1.68 ± 0.41%, and 3.11 ± 1.35% in patch stage ($n = 5$), plaque stage ($n = 10$), and tumor stage ($n = 3$), respectively. Also, the average percentages were 2.31 ± 0.76% (stage I, $n = 6$), 1.86 ± 0.49% (stage II, $n = 8$), and 2.71 ± 1.04% (stages III and IV, $n = 4$). There was no statistical correlation between CCR10 expression and the MF patient clinical stage. Immunohistochemical analysis for CCR10 in MF skin tissue also showed strong CCR10 expression in tumor cells (Fig. 4, top). Flow cytometric analysis for CCR10 in skin tissue was also investigated in skin tumor cells. CCR10 was markedly expressed in 34.03% of mononuclear cells (patient 16, tumor stage; Fig. 4, bottom). These results are consistent with a recent study (9).

Serum CTACK/CCL27 levels by ELISA. The serum CTACK/CCL27 concentrations in patients with MF were 993.6 ± 84.3 pg/mL. Conversely, those in healthy volunteers ($n = 9$) and atopic dermatitis patients ($n = 6$) were 430.6 ± 26.0 and 887.0 ± 56.9 pg/mL, respectively (Fig. 5, top). Serum CTACK/CCL27 levels were statistically elevated in patients with MF compared with normal controls ($P < 0.05$), but no statistical difference was found between patients with atopic dermatitis, in which the elevation of serum CTACK/CCL27 had been previously reported (15). Compared with each MF clinical stage, serum CTACK/CCL27 levels were 652.5 ± 28.3, 1,126.6 ± 111.7, and 1,118.7 ± 196.4 pg/mL during the patch ($n = 5$), plaque ($n = 10$), and tumor stages ($n = 3$), respectively. Statistically significant increases were found between the patch stage and the other two stages (Fig. 5, bottom). According to the tumor-node-metastasis classification, the average levels were 656.5 ± 23.5 (stage I, $n = 6$), 1,158.8 ± 125.0 (stage II, $n = 8$), and 1,169.0 ± 147.7 pg/mL (stages III and IV, $n = 4$). Patients with stage II or more advanced stages also showed a statistically higher level of serum CTACK/CCL27 than those with MF disease stage I ($P < 0.05$).

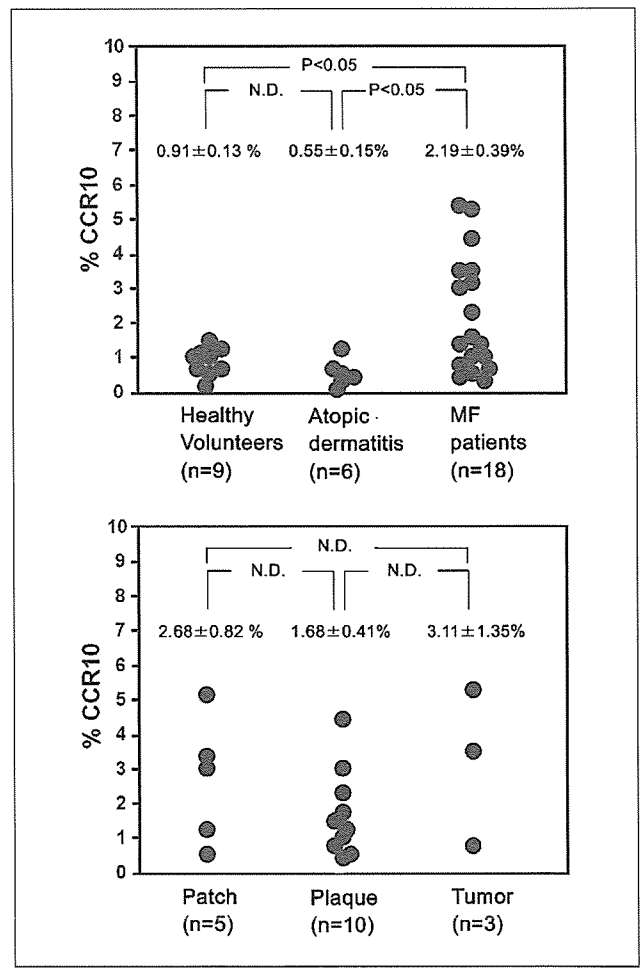

Fig. 3. CCR10 analysis using flow cytometry in PBMCs. *Top,* the percentage of CCR10+ T cells in PBMCs of MF patients were 0.55% to 5.3% (2.19 ± 0.39; average ± SE), which statistically exceeded those of healthy volunteers and patients with atopic dermatitis. *Bottom,* the expression of CCR10 was not correlated with MF clinical or disease stage.

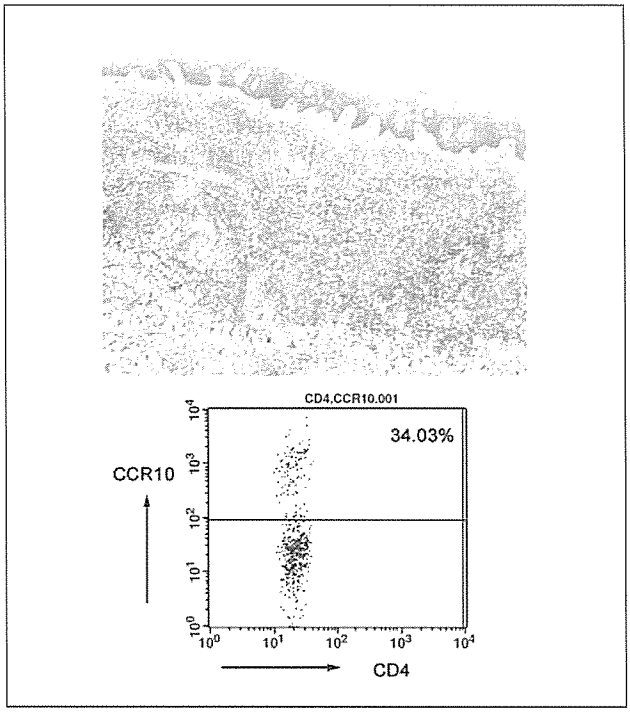

Fig. 4. CCR10 analysis in MF tumor tissues in patient 16. *Top,* marked CCR10 expression was noted in the abnormal infiltrated T cells (original magnification, ×50). *Bottom,* flow cytometric analysis also revealed increases in CCR10+ T cells within the lesional MF tissues.

Immunohistochemistry for CTACK/CCL27 in skin tissues. CTACK/CCL27 was strongly expressed in keratinocytes around both basal and suprabasal epidermal layers. CTACK/CCL27 diffusely stained the cytoplasm of keratinocytes (Fig. 6). In addition, endothelial cells of the superficial dermal plexus were stained. There was no correlation between the MF stages and extent of CTACK/CCL27 staining, or between serum CTACK/CCL27 levels and tissue expression (data not shown). Conversely, the CTACK/CCL27 expression in normal control skin was restricted to the basal cell layer (data not shown), as described previously (11).

Discussion

It has been shown that small numbers of clonal, aberrant T cells circulate in patients' peripheral blood even in early stages of MF, which is associated with the skipped expansion and micrometastasis of the MF lesions (3–5). In addition, circulating CLA+ CD4+ T cells express CCR10, a CC chemokine receptor for skin-homing function, in patients with CTCL (especially Sézary syndrome; ref. 8). Another study showed that malignant T cells in the MF lesional skin express CCR10 (9). Therefore, we speculate that CCR10 and its ligand CTACK/CCR27 play an important role in progression and skin-homing in early MF. In the present study, we have confirmed the previous findings in patients with MF, in addition to the following new observations: (*a*) we have identified significantly increased numbers of CCR10+ CD4+ cells is in MF patients' PBMCs without any other peripheral blood involvement as shown by routine laboratory tests, (*b*) CCR10 expression levels of individual circulating T cells do not vary according to MF disease stages, and (*c*) serum and skin CTACK/CCL27 are also elevated in patients with MF.

There is still the possibility that the CCR10 expression in our patients with MF is a reflection of inflammatory changes, as seen in atopic skin and in PBMCs of patients with severe drug reactions (11, 12). In fact, CCR10 is expressed by only 10% of CD4+ T cells in two models of inflammatory skin diseases (16), whereas it was expressed by 34% of MF lesion cells in our study. As shown in Fig. 3, there was no increase in CCR10 expression in atopic dermatitis cases. From these findings, we hypothesize that CCR10 is an important receptor involved in the pathophysiology of MF skin-homing and epidermotropism processes. In addition, the increase of CCR10+ CD4+ cells in the PBMCs of patients with MF is likely further proof that malignant, clonal T cells may already be circulating from early MF disease stages.

During skin-homing of peripheral T cells, chemokine interactions between CCR4, the thymus, and the activation-regulated

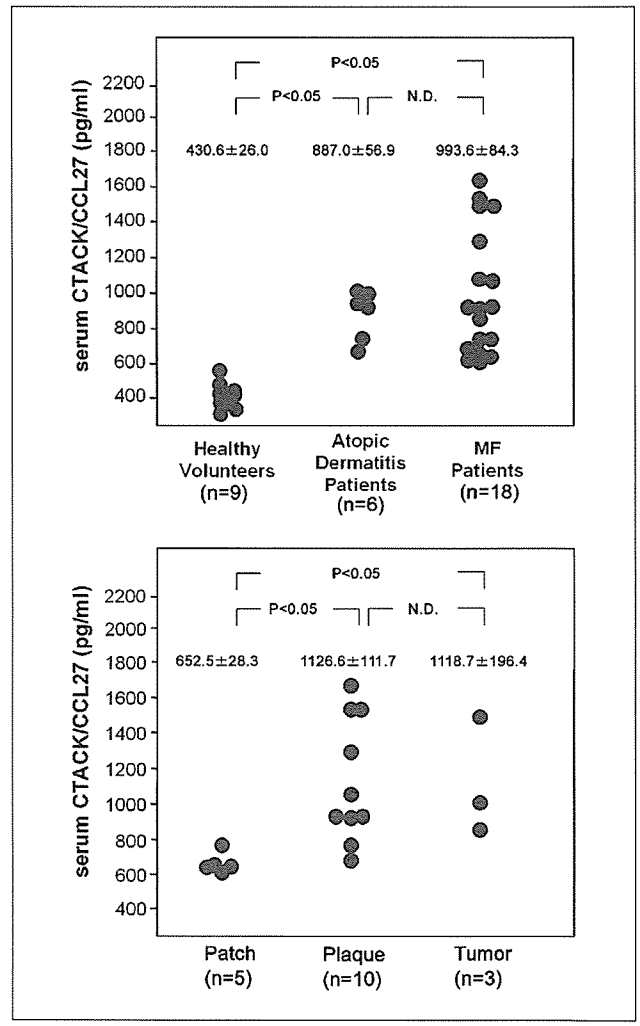

Fig. 5. Serum CTACK/CCL27 concentration assessed by ELISA. *Top,* both MF and atopic dermatitis patients have higher levels of CTACK/CCL27 than healthy volunteers. *Bottom,* a statistically significant elevation of serum CTACK/CCL27 levels was found between patch stage and other advanced stages.

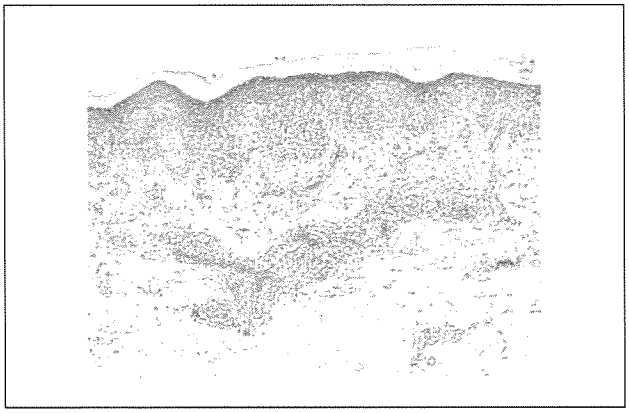

Fig. 6. Immunohistochemistry for CTACK/CCL27 in the MF skin tissue of patient 6 at the plaque stage. Generally, CTACK/CCL27 was expressed in suprabasal keratinocytes and endothelial cells of the superficial dermal plexus (original magnification, ×100).

chemokine (TARC/CCL17) have also been shown. Soler et al. reported that CCR10 is expressed only in a minor population of "effector-memory" skin-homing T cells, which respond to recently seen antigens (16). They also concluded that CCR10-CTACK interactions are not directly necessary for skin-homing, using anti-CTACK antibodies in the murine allergy model. Furthermore, CCR4 was expressed in other systemic cells than skin-homing T cells; hence, CCR10 might be more specific to the skin-homing population (11). Our study revealed that CCR10+ T cells were statistically elevated in patients with early MF than those from normal healthy controls or patients with atopic dermatitis, a common allergic skin reaction. Further studies are needed, but our study already suggests a role for CCR10-CTACK/CCR27 interactions during epidermotropism and skin-homing, not only in Sézary syndrome, but also in MF, by a subtly different pathway from other allergic skin reactions.

CTACK/CCL27, a functional ligand for CCR10, is predominantly expressed in basal keratinocytes of the epidermis (11). The concentration of CTACK/CCL27 around basal keratinocytes is rather high compared with other chemokines, playing a role in steady T cell trafficking into the skin (17). In our study, the serum CTACK/CCL27 concentration in patients with MF was significantly increased, which suggests a dynamic interaction between basal keratinocytes and malignant T cells.

Conversely, CCR4, another chemokine expressed by malignant T cells, also plays a central role in T helper 2–mediated cutaneous inflammation (18). A recent report revealed that TARC/CCL17, a ligand for CCR4, is significantly elevated in MF patients' serum, and that this is correlated with clinical and disease stages (19). It is also reported that TARC/CCL17 augments CTACK/CCL27 expression through tumor necrosis factor-α in atopic skin (20). These findings account for our observations that serum CTACK/CCL27 levels are elevated in patients with MF in accordance with the advance of the clinical stage. We believe that increases in the number of CCR10+ peripheral blood cells and serum CTACK/CCL27 levels may reflect the extent of increasing infiltration/inflammation during the course of the MF disease progress, as well as the importance of CCR4-TARC/CCL17 interactions during different disease stages.

A recent study has shown that single or multiple UV irradiation events can significantly down-regulate CTACK/CCL27 mRNA expression in mouse skin (21). Although no studies have been done to ascertain the relationship between CCR4 expression and UV therapy, one CTCL case has been reported in which the numbers of peripheral CCR4+ malignant T cells significantly decreased after retinoid plus psoralen UV A and IFN-γ therapy (22). These findings may explain one mechanism by which PUVA might be effective in treating CTCL skin lesions, by decreasing the affinity of skin-homing T cells and their rates of infiltration.

In summary, we have found that the CCR10+ CD4+ lymphocytes are significantly increased in the circulating PBMCs of patients with MF, regardless of clinical disease progression. An elevated concentration of serum CTACK/CCL27 was also noted in patients with MF, which together suggests an increase in lymphocyte skin-homing in the early stages of MF.

Acknowledgments

We thank Dr. James R. McMillan for critical proofreading of this manuscript.

References

1. Weinstock M, Horm J. Mycosis fungoides in the United States: increasing incidence and descriptive epidemiology. JAMA 1988;260:42–6.
2. Willemze R, Jaffe ES, Burg G, et al. WHO-EORTC classification for cutaneous lymphomas. Blood 2005;105:3768–85.
3. Washington LT, Huh YO, Powers LC, Duvic M, Jones D. A stable aberrant immunophenotype characterizes nearly all cases of cutaneous T-cell lymphoma in blood and can be used to monitor response to therapy. BMC Clin Pathol 2002;2:5.
4. Heald PW, Yan SL, Edelson RL, Tigelaar R, Picker LJ. Skin-selective lymphocyte homing mechanisms in the pathogenesis of leukemic cutaneous T-cell lymphoma. J invest Dermatol 1993;101:222–6.
5. Muche JM, Lukowsky A, Asadullah K, Gellrich S, Sterry W. Demonstration of frequent occurrence of clonal T cells in the peripheral blood of patients with primary cutaneous T-cell lymphoma. Blood 1997;90:1636–42.
6. Ferenczi K, Fuhlbrigge RC, Pinkus J, Pinkus GS, Kupper TS. Increased CCR4+ expression in cutaneous T cell lymphoma. J Invest Dermatol 2002;119:1405–10.
7. Campbell JJ, Haraldsen G, Pan J, et al. The chemokine receptor CCR4 in vascular recognition by cutaneous but not intestinal memory T cells. Nature 1999;400:776–80.
8. Sokolowska-Wojdylo M, Wenzel J, Gaffal E, et al. Circulating clonal CLA+ and CD4+ T cells in Sézary syndrome express the skin-homing chemokine receptors CCR4 and CCR10 as well as the lymph node-homing chemokine receptor CCR7. Br J Dermatol 2005;152:258–64.
9. Notohamiprodjo M, Segerer S, Huss R, et al. CCR10 is expressed in cutaneous T-cell lymphoma. Int J Cancer 2005;115:641–7.
10. Morales J, Homey B, Vicari AP, et al. CTACK, a skin-associated chemokine that preferentially attracts skin homing memory T cells. Proc Natl Acad Sci U S A 1996;96:14470–5.
11. Homey B, Alenius H, Muller A, et al. CCL27-10 interactions regulate T cell-mediated skin inflammation. Nat Med 2002;8:157–65.
12. Tapia B, Padial A, Sanchez-Sabate E, et al. Involvement of CCL27-10 interactions in drug-induced cutaneous reactions. J Allergy Clin Immunol 2004;114:335–40.
13. Reiss Y, Proudfoot AE, Power CA, Campbell JJ, Butcher EC. CC chemokine receptor (CCR) 4 and the CCR10 ligand cutaneous T cell-attracting chemokine (CTACK) in lymphocytic trafficking to inflamed skin. J Exp Med 2001;194:1541–7.
14. Kashani-Sabet M, McMillan A, Zackheim HS. A modified staging classification for cutaneous T-cell lymphoma. J Am Acad Dermatol 2001;45:700–6.
15. Hon KL, Leung TF, Ma KC, Li AM, Wong Y, Fok TF. Serum levels of cutaneous T-cell attracting chemokine (CTACK) as a laboratory marker of the severity of atopic dermatitis in children. Clin Exp Dermatol 2004;29:293–6.
16. Soler D, Humphreys TL, Spinola SM, Campbell

JJ. CCR4 versus CCR10 in human cutaneous Th lymphocytic trafficking. Blood 2003;101: 1677–83.

17. Bäumer W, Seegers U, Braun M, Tschernig T, Kietzmann M. TARC and RANTES, but not CTACK, are induced in two models of allergic contact dermatitis. Effects of cilomilast and diflorasone diacetate on T-cell-attracting chemokines. Br J Dermatol 2004; 151:823–30.

18. Vestergaard C, Bang K, Gesser B, Yoneyama H, Matsushima K, Larsen CG. A Th2 chemokine, TARC, produced by keratinocytes may recruit CLA+ CCR4+ lymphocytes into lesional atopic dermatitis skin. J Invest Dermatol 2000;115: 640–6.

19. Kakinuma T, Sugaya M, Nakamura K, et al. Thymus and activation-regulated chemokine (TARC/CCL17) in mycosis fungoides: serum TARC levels reflect the disease activity of mycosis fungoides. J Am Acad Dermatol 2003;48:23–30.

20. Vestergaard C, Johansen C, Christensen U, Just H, HohwyT, Deleuran M. TARC augmentsTNF-α-induced CTACK production in keratinocytes. Exp Dermatol 2004;13:551–7.

21. Rundhaug JE, Hawkins KA, Pavone A, et al. SAGE profiling of UV-induced mouse skin squamous cell carcinomas. comparison with acute UV irradiation effects. Mol Carcinog 2005;42:40–52.

22. Fujimura T, Aiba S, Yoshino Y, et al. CCR4 Expression by atypical T cells in systemic pilotropic lymphoma: its behavior under treatment with interferon γ, topical PUVA and systemic retinoid. Dermatology 2004;208: 221–6.

Nail dystrophy and blisters as sole manifestations in myeloma-associated amyloidosis

Yasuyuki Fujita, MD,[a] Yukiko Tsuji-Abe, MD,[a] Kazuko C. Sato-Matsumura, MD, PhD,[b] Masashi Akiyama, MD, PhD,[a] and Hiroshi Shimizu, MD, PhD[a]
Sapporo, Japan

We report the case of a 61-year-old Japanese man with IgG λ-type multiple myeloma, who presented with nail dystrophy as the initial manifestation of systemic amyloidosis. Subsequently he developed bullous amyloidosis. This report documents these two rare signs of systemic amyloidosis and demonstrates the precise location of cutaneous blister formation and amyloid deposition by fluorescence antigen mapping and electron microscopy. (J Am Acad Dermatol 2006;54:712-4.)

Systemic amyloidosis develops in approximately 15% of multiple myeloma patients, and between 29% and 40% of the patients develop mucocutaneous disease.[1] Common cutaneous symptoms include "pinch" purpura, waxy papules, nodules, plaques, and macroglossia. Nail dystrophy and cutaneous blisters are rare.[1] We report a case of systemic amyloidosis associated with multiple myeloma; the patient presented with only two of the rarer cutaneous manifestations, nail dystrophy and blisters, without any other visceral dysfunction usually seen in systemic amyloidosis. Furthermore, we demonstrate the precise location of blister formation by immunofluorescence mapping and electron microscopy.

CASE REPORT

A 61-year-old Japanese man with a 4-year history of nail dystrophy was referred to us. His medical history was significant for IgG-λ− type multiple myeloma of 7 years' duration, with a poor response to combination chemotherapy and autologous peripheral blood stem cell transplantation. Physical examination revealed thin, brittle nail plates with longitudinal ridging and onychoschizia on all 10 fingernails and his great toenails (Fig 1, *A*). Dermatophytes and *Candida* organisms were not detected after microscopic examination and fungal culture. No other mucocutaneous abnormalities were identified.

A biopsy specimen from the nail bed of his right forefinger demonstrated eosinophilic, amorphous deposits within the dermal papilla and in the dermal perivascular regions (Fig 1, *B*). These deposits were positive for Congo red and direct fast scarlet staining (Fig 1, *C*). The diagnosis of nail dystrophy associated with systemic amyloidosis was made. Further investigations for visceral disease, including a urine test, electrocardiography, and computed tomography, yielded unremarkable results.

Fourteen months later, tense, painful vesicles measuring up to 1 cm developed on the patient's forearms (Fig 1, *D*). Mild mechanical friction easily induced new blister formation, indicating severe skin fragility. A skin biopsy specimen from a new blister demonstrated subepidermal separation and eosinophilic, amorphous deposits in the dermal papilla (Fig 1, *E*). These deposits were positive for Congo red and direct fast scarlet staining with resistance to potassium-permanganate, indicating amyloid light chain–type amyloid deposition (Fig 1, *F*). No autoantibodies were detected by means of direct and indirect immunofluorescence.

To investigate the precise location of blister formation and amyloid deposition, we examined the specimens with fluorescence antigen mapping. Type IV collagen (CIV 22, Lab Vision, Newmarket, UK), a molecule present in the lamina densa, was detected on the blister floor (Fig 2, *A*). Conversely, β_4 integrin (3E1, Chemicon International Inc, Temecula, Calif), a hemidesmosome transmembrane protein subunit of the α_6/β_4 integrin, mapped to the blister roof (Fig 2, *B*). These findings indicated the blister location within the lamina lucida.

From the Departments of Dermatology, Hokkaido University Graduate School of Medicine[a] and Sapporo Social Insurance General Hospital.[b]

Funding sources: None.

Conflicts of interest: None identified.

Reprint requests: Yasuyuki Fujita, MD, Department of Dermatology, Hokkaido University Graduate School of Medicine, N15 W7, Kita-ku, Sapporo, Hokkaido 060-8638, Japan. E-mail: yfujita@med.hokudai.ac.jp.

0190-9622/$32.00

doi:10.1016/j.jaad.2005.12.031